## Abstract

FICARRA, CHRISTINA HELENE. Analysis of adhesive bonded fiber-reinforced composite joints. (Under the direction of Dr. Eric Klang.)

The work presented in this thesis involved the analysis of adhesive bonded joints for composite bridge decks and was divided into three phases. The first phase involved a parametric study on a single lap joint using ANSYS finite element analysis software. The purpose of the parametric study was to alter the geometry and material properties of the joint and study their effects on the stress distribution in both the adherends and adhesive. The four different cases studied included adding a taper to the adherends, different edge shapes on the adhesive layer, a material stiffness imbalance and a geometric stiffness imbalance.

It was found that for the taper case and the edge shape case, the stress field in the joint was affected slightly. The material and geometric stiffness imbalance cases had the most drastic affect on the stress field of both the adhesive and adherend.

Phase two of this study involved physical tests on single lap joints pulled in uniaxial tension. Tests were performed on three different types of laminates in order to study the interfacial effects these laminates had on the adhesive bond. It was found that by changing the surface of the composite, the mode of failure changed significantly.

Phase three of this research involved a study on surface preparation. Three different surface preparations were conducted on the adherends of a butt-strap joint. The first included an acetone wipe. The second involved sanding the adherends. The third surface preparation involved adding APRIME-2, a secondary bonding agent, to the adherends before adding the strap. By simply sanding the adherends, the load to failure

was increased by 350% compared to an acetone wipe. The ATPRIME-2 improved the load to failure by an additional 60% as well as improved the failure mode to a fiber tear. It was concluded that surface preparation has a major impact on the behavior of adhesively bonded joints.

# ANALYSIS OF ADHESIVE BONDED FIBER-REINFORCED COMPOSITE JOINTS

by

**Christina Helene Ficarra**

A thesis submitted to the Graduate Faculty of
North Carolina State University
in partial fulfillment of the
requirements for the Degree of
Master of Science

**Department of Mechanical and Aerospace Engineering**

Raleigh

2001

**Approved by:**

_____ _____

_____
Chairman of Advisory Committee

## Dedication

I would like to dedicate this paper to my dad. Without his amazing support and love I would never have been able to complete this.

I would also like to dedicate this to my mom. During her short time on earth she introduced me to the greatest teacher of all, Jesus Christ.

## Biography

Christina was born and raised in New York as the youngest of four children to Joe and Lorraine Ficarra. In 1999 she graduated from Messiah College and moved down south to begin her graduate studies at NC State. Throughout her two years in Raleigh, she learned engineering theory, attended her first pig pickin' and developed a love for sweet tea.

## Acknowledgements

I would like to thank the following people:

Dr. Klang for his tremendous help and guidance throughout these past two years.

Dr. Dan Richards at Martin Marietta Composites for making this project possible.

My committee members, Dr. Eischen and Dr. Silverberg for their support with this research.

David Motley for his unending help in preparing this paper and conducting the experiments.

Tom, Carol, Katie, Rachel and Tommy Mercer for giving me a family in North Carolina.

Last, I would like to thank Adam Curry, whose incredible love and friendship carried me through the last year of school.

# Table of Contents

# List of Tables

## List of Figures

# 1. Introduction

For over 50 years, fiber-reinforced plastic (FRP) materials have proven to be very successful in structural applications. They are widely used in the aerospace, automotive and marine industries. One area of application that has benefited greatly from the use of FRP is the design and rehabilitation of highway concrete bridge decks. Some advantages of a FRP bridge deck include:

- Less than one-fifth the weight of a comparable concrete slab
- High corrosion resistance
- High fatigue resistance
- High strength-to-weight ratio
- Ease of installation due to lightweight equipment
- Low maintenance cost
- Superior life-cycle cost-effectiveness

FRP materials, or composites, behave differently than typical metals such as steel or aluminum. A typical composite contains layers of aligned fibers oriented at different angles held together by a resin matrix, giving it high stiffness and strength in different directions. This anisotropy can cause difficulties when joining two parts together, especially if the two pieces have different stiffness and strength characteristics. The joint can potentially become the weakest link in the structure due to the large amount of load it must transfer.

There are a wide variety of ways to join different parts together. Two major methods include mechanical fastening and adhesive bonding. While mechanical fastening

has some advantages such as ease of disassembly, it can create significant stress risers in composites. These stress risers can weaken the overall strength of the structure. For bolted or riveted joints, it is often necessary to bond a load-spreading insert onto the composite so that the load is diffused into the structure less abruptly. On the other hand, an adhesive bond can transfer the load from one piece to another without creating a significant stress concentration. While there are some limitations to an adhesively bonded joint, it is one if the preferred methods of joining composite parts. Table 1.1 illustrates the advantages and disadvantages of an adhesive bond.

**Table 1.1: Advantages and Disadvantages of an adhesively bonded joint**

| Advantages | Disadvantages |
|---|---|
| Uniform load distribution | Joints cannot be disassembled |
| Minimal stress concentrations | Bond performance dependent upon surface preparation |
| Able to bond dissimilar materials | Bond performance affected by environmental effects |
| Surface is smooth and without protrusions from bolts, etc. | rone to environmental degradation<br>ifficult to verify the bondline |

Some of the more common types of adhesive joints include a single lap, double lap, butt strap, tube and scarf joint.

This research was conducted in conjunction with Martin Marietta Composites (MMC) and focused on adhesive bonds involving their Duraspan$^{TM}$ FRP composite bridge deck. The FRP bridge deck concept began in 1992 with Lockheed Martin Missiles

& Space Company at the Palo Alto Research and Development Laboratory. In 1995, Lockheed Martin sold the technology to its spin-off company, Martin Marietta Materials. Martin Marietta Composites (MMC) was then created to manage and promote the deck. MMC has since installed several decks across the United States.

The bridge decks are manufactured by means of pultrusion, which involves wetting the layered fabric in a polyester resin bath and pulling it through a heated die to form long, dual-celled tubes. The tubes are then bonded together in ten-foot panel sections with polyurethane adhesive prior to being shipped to the installation site. Figure 1.1 depicts four tubes bonded together.

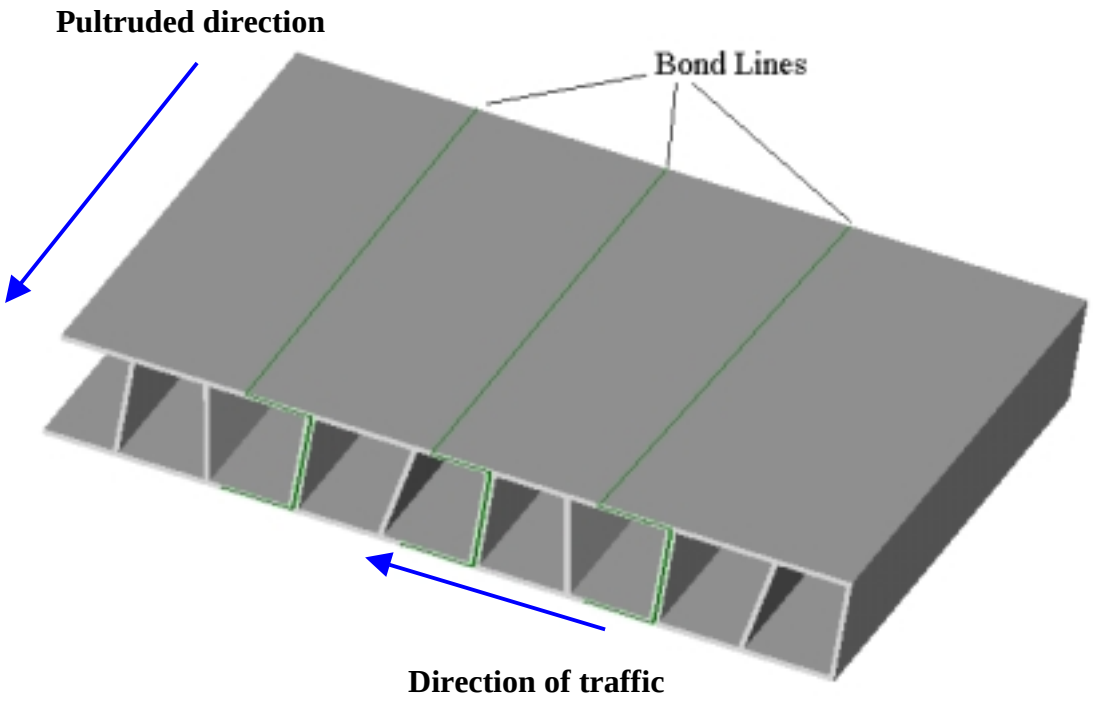


***Figure 1.1: Schematic of Duraspan™ Deck Panel***

Once the panels arrive on site, they are bonded together by field joints to form the entire deck. These field joints, or splices, are created by first adding a liquid primer to both sides of the joint, then an epoxy paste. The panels are then lowered and jacked into place. FRP dowel bars are installed in the lips of the joints so that the bond line remains secure while curing. Once the bond line has cured, FRP splice strips are installed over the joints to ensure a watertight and durable joint. This process is illustrated in figure 1.2.

(a) Application of primer and epoxy

(b) Panels lowered into place

(c) FRP dowels installed

(d) FRP splice strips installed

***Figure 1.2: Installation of MMC FRP bridge deck***

A completed bridge is shown in figure 1.3.

***Figure 1.3: Completed bridge***

This type of joint is just one of the different types of structural splices needed in a FRP bridge deck. Often it is necessary for larger bridges to include a crown down the center of the bridge deck for water runoff. In order to create a crown in the Duraspan™ FRP decks, the tubes need to be cut perpendicular to the pultruded direction (see figure 1.1), angled down 2 degrees from each other, then bonded back together again.

## 1.1 Purpose and Scope

The purpose of this research was to investigate the behavior of a FRP composite single lap adhesively bonded joint. This information will aid in the design of a structural splice for the MMC FRP bridge deck. This was accomplished by first creating an accurate finite element model that would analyze an adhesively bonded joint for a parametric study. In this study, the geometry and material properties were altered in order to determine their effects on the overall behavior of the joint. Then, physical tests using different adhesives and laminates were conducted in order to study the bond line interface

and mode of failure of the joints. Finally, a study on surface preparation was carried out on a butt-strap joint to determine how that affects the adhesive bond.

# 2. Background

A significant amount of research has been dedicated to the study of adhesive bonded joints. An exact solution for the stress field of these joints is difficult to obtain due to the geometric complexity and material non-linearity of the adhesive. This has resulted in a wide range of solutions developed, each with different assumptions and simplifications. For simplicity, this investigation of the various stress analysis methods has been limited to a single lap joint. Figure 2.1 shows the geometry and terminology of a single lap joint.

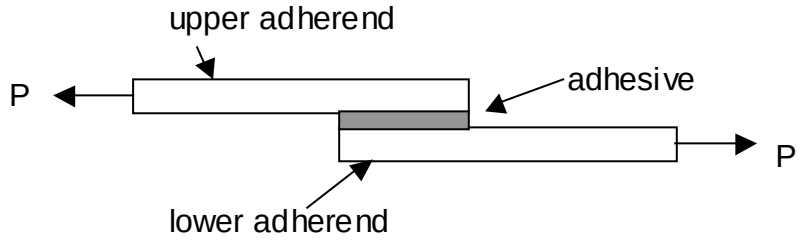


***Figure 2.1: Single Lap Joint***

The most basic analysis of an adhesive includes a linear elastic solution derived from mechanics of materials. The adherends are assumed to be rigid, while the adhesive deforms only in shear. The shear stress is given by:

$$\tau = \frac{P}{bl} \tag{2.1.1}$$

Where $P$ is the applied load, $b$ is the width and $l$ is the length of the overlap. The shear stress is assumed to remain constant along the joint length. While equation (2.1.1)

provides a baseline average shear stress in the adherends under loading, it is not accurate for determining the stresses in the adhesive.

V.O. Volkersen [2] pioneered the investigation into analyzing the stress field in an adhesive joint with his shear lag analysis. One major aspect of his work was to analyze the non-uniform deformation of the adhesive layer under loading known as *differential shear*. Goland and Reissner [3] expanded on Volkersen's work by including the effects of the bending moment applied to the joint under tensile loading due to the adherends being non-colinear. L.J. Hart-Smith [4] takes this analysis a step further by taking into account the plasticity of the adhesive. This paper concentrates on the analysis developed by V.O. Volkersen, Goland and Reissner and L.J. Hart-Smith. Details of their work are described in chapters 3 and 4. Following are examples of other methods for determining the stresses in a bonded joint that have been developed over the years.

The analysis of Klarbring and Movchan [5] involved mathematically modeling the adhesive joint using an asymptotic approach. They assumed the joint to be an elastic beam with three layers, the middle being infinitesimally thin and soft compared to the two outer layers. The approach is not based on strength of materials assumptions, but rather the rigorous asymptotic analysis of the Lamé system in thin regions. While this method is efficient for deriving equations for compound structures, no correlation with physical data was presented.

Delale and Erdogan [6] analyzed a single lap joint by assuming the adherends to be linear elastic and the adhesive to be linearly viscoelastic. The standard Laplace transform technique was implemented to solve the problem. Their results indicated that the

maximum normal stress in the adhesive is consistently higher than the corresponding shear stress and decays slower.

Frostig et al. [7] developed a closed-form higher-order theory (CFHO) for the analysis of adhesive bonded joints. This approach satisfies the boundary/continuity conditions in the adhesive layer at the edge of the overlap. This differs from the Goland-Reissner type solutions that only satisfy these conditions globally. This will be explained in greater detail in chapter 3. It also assumes that transverse normal stresses are not uniform through the thickness. These factors allow for the adhesive layer to fulfill point, as well as global equilibrium. The governing equations for this theory have been derived assuming that the adherends are linearly elastic composite laminates and the adhesive layer is homogeneous, isotropic and linear-elastic. Good agreement was found with a comparable finite element solution and a Goland and Reissner solution for both a square edge and a fillet at the edge of the overlap in the adhesive. However, because the non-linearity in the adhesive was not taken in to account, the results will predict a higher stress than actually exists.

Adams and Peppiatt [8] analyzed a bonded joint using a two-dimensional linear elastic finite-element method. The problem was assumed to be one of plane strain. Significant attention was given to the edge effects of the adhesive. Rather than simplifying the edge to be a square, a triangular fillet was used. The shape of the fillet was verified by experiments performed using a rubber model. A parametric study on the size of the triangular fillet revealed that the edge stresses could decrease by as much as

30% as compared to a square edge. This reduction in edge stresses has a significant effect on the overall joint strength.

While the assumption that composite adherends have linear elastic behavior is fairly accurate, geometric nonlinearity needs to be taken into account, especially in a single lap joint. For this type of joint, as the load is applied, the adherends will tend to rotate due to eccentricity of the load path. Depending on the thickness of the adherend, this rotation can be very large, making the problem geometrically non-linear. Dattaguru et al [9] performed a 2-dimensional plane stress finite-element analysis for a bonded joint taking into account this type of nonlinearity. Their analysis found that these rotations significantly affected the mode I and II strain-energy-release rates. In order to accurately capture the stress state in the adhesive, it is important to include this geometric nonlinearity.

# 3. Elastic Analysis of a Single Lap Joint

## 3.1 Volkersen's Shear Lag Analysis

The basic stress distribution given by equation (2.1.1) assumes the adherends to be rigid and the adhesive to deform only in shear. The tensile stress in the upper adherend will decrease linearly to zero from point A to point B. The converse is true for the lower adherend. Therefore the shear stress in the adhesive bond is constant, as shown in Figure 3.1(a). Note how the parallelograms are uniformly sheared.

However, if the adherends are allowed to deform elastically, the adhesive shear stress distribution is dramatically different as shown in figure 3.1(b). For the upper adherend, the tensile stress is at a maximum at A and falls to zero at B, but not linearly. The converse is true for the lower adherend. Because the stress is at a maximum at A, the tensile strain at A is larger than at B and is reduced along the length of the bond line. This causes the parallelograms in figure 3.1(a) to become distorted as shown in figure 3.1(b). This distortion results in a non-uniform shear stress distribution along the adhesive/ adherend interface with peak stresses at the ends of the joint

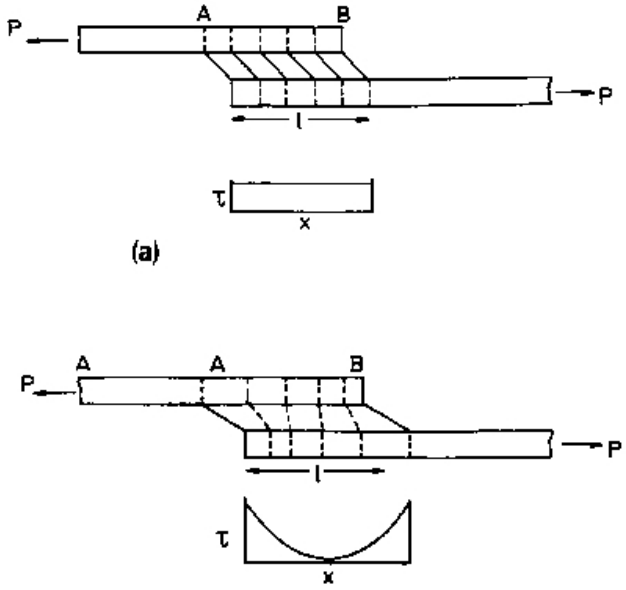


***Figure 3.1: Deformations of a single lap joint: (a) with rigid adherends; (b) with elastic adherends [1]***

V.O. Volkersen studied this phenomenon, termed differential shear, and in 1938 presented his shear lag analysis. In this analysis he assumed that the adhesive deforms only in shear, the adherends deform only in tension, and both the adhesive and adherends are linearly elastic. The adhesive shear stress distribution is given as:

$$\tau = \frac{\omega}{2}\frac{\cosh \omega X}{\sinh \omega/2} + \left(\frac{\psi - 1}{\psi + 1}\right)\frac{\omega}{2}\frac{\sinh \omega X}{\cosh \omega/2} \tag{3.1.1}$$

Where

$$\omega^2 = (1 - \psi)\phi \tag{3.1.2}$$

$$\psi = \frac{t_1}{t_2} \tag{3.1.3}$$

$$\phi = \frac{Gl^2}{Et_1t_3} \tag{3.1.4}$$

$$X = \frac{x}{l} \tag{3.1.5}$$

In the above equations, $t$ is the thickness, $G$ is the adhesive shear modulus, $E$ is the Young's modulus of the adherends and $l$ is the length of the overlap. Subscripts 1, 2 and 3 are the two adherends and adhesive layer respectively.

While this method provides a classical elastic solution to the adhesive shear stress distribution in a single lap joint, it is not supported by experimental results. Volkersen did not take into account two important factors in his shear lag analysis. First, in a single-lap joint, the directions of the two forces are not collinear. Rather, the line of action of the load path is eccentric. This results in a bending moment applied to the joint as well as the in-plane tension. This eccentricity also gives rise to transverse normal or peeling stresses, which play a significant role in the mode of failure of the joint. Second, because the adherends bend, the joint rotates and the joint displacements are no longer proportional to the applied load. If this angel of rotation is large, the problem becomes geometrically nonlinear.

## 3.2 Goland and Reissner

In the 1940's, Goland and Reissner [6] improved Volkersen's analysis by including the deflection of the joint due to the bending moment and the peel stresses. Their stress analysis was divided into two parts. The first part involved determining the loads at the

edges of the joint. The second part dealt with determining the stresses in the joint due to the applied load. Their assumptions were the following:

- The normal stress parallel to the layer in the adhesive is neglected
- All other normal stresses in the adhesive do not vary across the thickness
- The problem is one of plane strain

By using strain energy methods and the above assumptions, they derived the overall strain energy in the joint. By minimizing the strain energy equation, the correct stress distribution, which satisfies equilibrium and the boundary conditions, was established for two limiting cases.

The first case assumes that the adhesive layer is very thin compared to the adherends and that all flexibility is due to the adherends. This case is also valid for relatively thick adhesive layers whose material properties are of the same order of magnitude as the adherends. The limiting values are:

$$\frac{t_3 E_1}{t_1 E_3} \leq 0.1 \quad \text{and} \quad \frac{t_3 G_1}{t_1 G_3} \leq 0.1 \tag{3.2.1}$$

The second case assumes that the adhesive layer is relatively thick compared to the adherends and that all flexibility is due to the adhesive. The limiting values are:

$$\frac{t_1 E_3}{t_3 E_1} \leq 0.1 \quad \text{and} \quad \frac{t_1 G_3}{t_3 G_1} \leq 0.1 \tag{3.2.2}$$

Most practical joints fall outside the bounds of case 2. However, Lubkin and Reissner later found that the bounds are conservative after conducting photoelasticity experiments. No indication was given of the true bounds of the equations. Limitations of this theory include the inability to control the boundary and continuity conditions of the adhesive

layer at the edges of the overlap. Because of this, the stress fields in the adhesive maintain global equilibrium, but not point equilibrium. This method is therefore accurate enough to determine the stress distributions in a global sense, but does not capture the local stress behavior in the adhesive. The shear stress distribution of Goland and Reissner is given by:

$$\tau_0 = \left(-\frac{1}{8}\right)\left(\frac{pt_1}{c}\right)\left[\frac{\beta c}{t_1}(1+3k)\frac{\cosh\left(\frac{\beta}{t_1}\frac{x}{c}\right)}{\sinh\left(\frac{\beta c}{t_1}\right)}+3(1-k)\right] \tag{3.2.3}$$

Where

$$\beta^2 = 8\frac{G_3}{E_1}\frac{t_1}{t_3} \tag{3.2.4}$$

The transverse normal, or peel stress distribution is given by:

$$\sigma_0 = \frac{pt^2}{c^2R^3}\left[\begin{array}{l}\left(R_2\lambda^2\frac{K}{2}-\lambda K'\cosh\lambda\cos\lambda\right)\cosh\frac{\lambda x}{c}\cos\frac{\lambda x}{c}+\\ \left(R_1\lambda^2\frac{K}{2}-\lambda K'\sinh\lambda\sin\lambda\right)\sinh\frac{\lambda x}{c}\sin\frac{\lambda x}{c}\end{array}\right] \tag{3.2.5}$$

Where

$$\lambda = \gamma\frac{c}{t_1} \tag{3.2.6}$$

$$\gamma^4 = 6\frac{E_3}{E_1}\frac{t_1}{t_3} \tag{3.2.7}$$

$$K' = K\frac{c}{t_1}\left[3\left(1-\nu^{2}\right)\frac{p}{E_1}\right]^{\frac{1}{2}} \tag{3.2.8}$$

$$c = \frac{l}{2} \tag{3.2.9}$$

$$R_1 = \cosh\lambda \sin\lambda + \sinh\lambda \cos\lambda \tag{3.2.10}$$

$$R_2 = \sinh\lambda \cos\lambda - \cosh\lambda \sin\lambda \tag{3.2.11}$$

$$R_3 = \frac{\sinh 2\lambda + \sin 2\lambda}{2} \tag{3.2.12}$$

Figure 3.2 shows a comparison of shear stress distribution between Volkersen's shear lag analysis and Goland and Reissner's second case. The adherends are 4.0 inches long by 1.0 inch wide and have a thickness of 0.5 inches. The bonded area was 1.0 inch wide by 1.0 inch long with an adhesive thickness of 0.03 inches. The material properties were taken from table 3.1. The applied load was 2000 lbs. In figure 3.2, the center of the adhesive bondline is at x= 3.5.

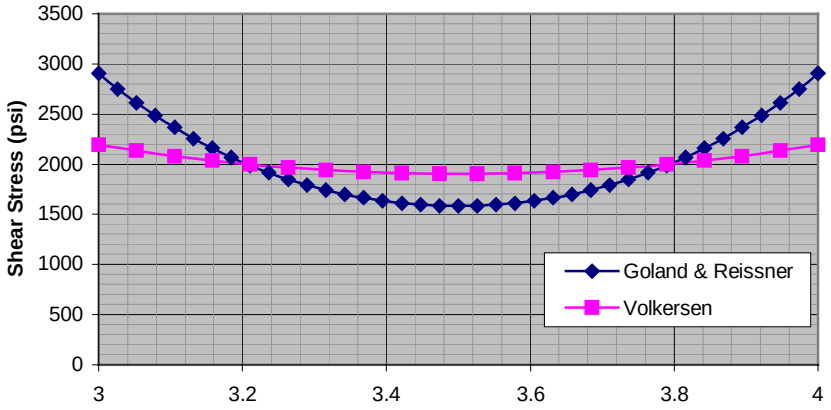


***Figure 3.2: Comparison between shear stress distribution of Volkersen and Goland & Reissner for an applied load of 2000 lbs.***

The solution of Goland and Reissner matched experimental results more accurately than Volkersen's solution.

## 3.3 FEA- Elastic Solution

Using ANSYS software, a finite element analysis was performed on a single lap joint. The model was verified by ensuring that the trends of the stress distribution in the adhesive agreed with Goland and Reissner's theory. However, a complete match was not expected due to the assumptions and simplifications built into Goland and Reissner's analysis that are not included in a numerical analysis. These differences will be explained in more detail later.

Three main cases were investigated for an elastic analysis. One case modeled the adherends and adhesive with Solid45 elements. These are three dimensional, eight node structural solid elements. The second and third cases modeled the adherends and

adhesives using two dimensional, four node Plane42 elements in plane strain and plane stress, respectively. Recall that plane strain assumes the width approaches infinity while plane stress assumes the width to be very small. While a single lap joint can be modeled easily using plane elements, a typical joint falls somewhere in between these two extremes. Therefore a solid FEA model was created to investigate the effects of the actual width of the joint on the stress distribution.

In order to accurately capture the adhesive stress distribution, an extremely fine mesh is required along the adhesive bond line. For plane elements, a finer mesh can be generated and the solution can be solved for fairly quickly. This is not the case for the solid elements.

The adhesive properties modeled in the finite element analysis came from PLIOGRIP Structural Adhesive provided by Ashland Chemical. The MMC composite adherend properties were taken from tests performed by Delsen Testing Laboratories, Inc. [10]. The material properties for both the composite and adhesive are listed in table 3.1.

**Table 3.1: Adhesive and adherend material properties**

| *Material Property* | *PLIOGRIP adhesive* | *MMC composite* |
|---|---|---|
| Ex (ksi) | 75 | 2160 |
| Ey (ksi) | 75 | 1500 |
| Ez (ksi) | 75 | 3940 |
| Poisson's ratio | 0.4 | 0.28 |

### 3.3.1 FEA Elastic Solution: Solid Model

A three-dimensional solid finite element model was created first. The geometry of the single lap joint was taken from actual lap shear tests performed at North Carolina State University. Details of these physical tests will be explained later. The adhesive was modeled with a width of 1.0 inch, a length of 1.0 inch and a thickness of 0.03 inches. The adherends were both 4.0 inches long, 1.0 inch wide and 0.5 inches thick. The overlap length of the bond was 1.0 inch. Figure 3.3 illustrates the geometry, boundary and loading conditions of the solid model. The adhesive edges were modeled as square. In reality, some of the adhesive is squeezed out of the joint during manufacturing, forming a rounded fillet at the edge. For simplicity, this fillet was not included in the model.

A distributed load of 1000 lbs was applied to the top and bottom edge nodes of the lower adherend to simulate a 2000 lb static load on the joint. The vertical translation was constrained along the top and bottom nodes of both adherends for 0.5 inches along the length starting at the free edges. This represented the constraints applied by the grips in the actual testing machine.

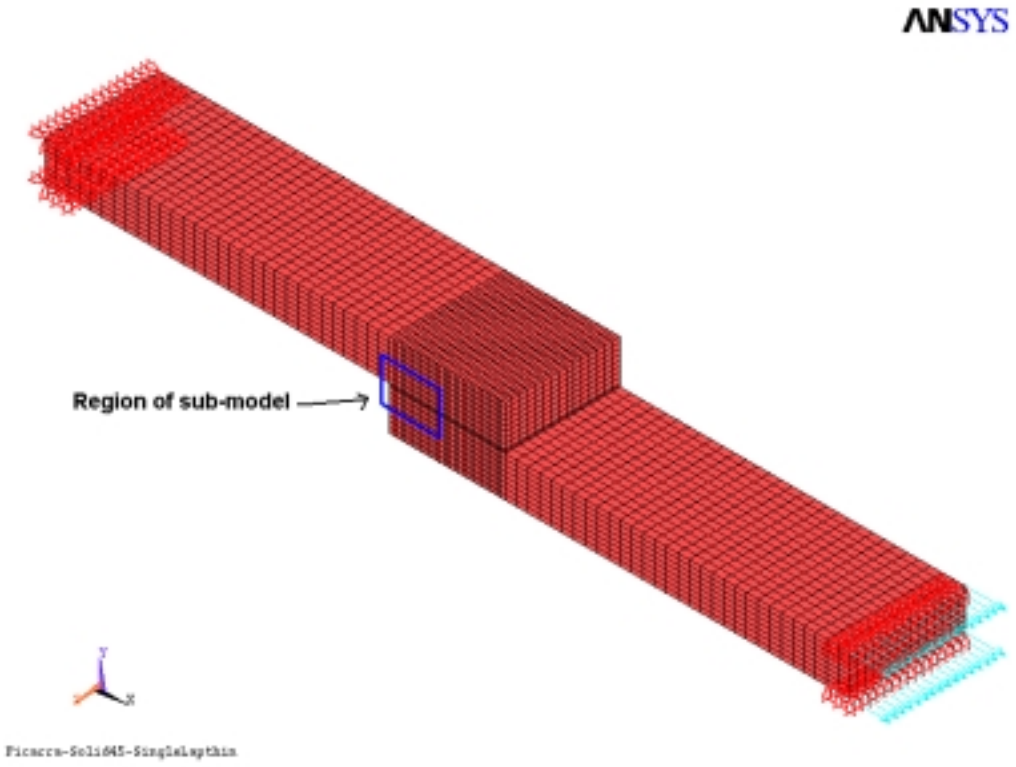


***Figure 3.3: Geometry, loading and boundary conditions for the solid45 element modeled***

The mesh was refined in the overlap area to capture the correct stress state in the adhesive. However, as more elements were created in the model, the computer processing time increased significantly. Therefore the degree of refinement was limited. In order to increase the accuracy of the solution, a sub-model of a portion of the bond was created.

Before the sub-model could be analyzed, the full model was analyzed to acquire the proper boundary conditions along the sub-modeled region boundary. Then, this region was pulled out of the full model, the mesh was refined, and the boundary conditions from the large analysis were attached to the proper edges. The sub-modeled

region is outlined in blue in figure 6 and included 32718 nodes and 27200 elements. Note that the sub-model included the width of the joint (not indicated on the figure).

Because this is a three-dimensional numerical solution of the single lap joint, an exact agreement with Goland and Reissner's solution was not expected. Their assumptions of plane strain and negligible normal stresses in the adhesive layer were not incorporated into the FEA model. However, a similar pattern in the stress distribution was observed. Figures 3.4 and 3.5 compare the adhesive peel and shear stress distribution of the full FEA model, sub-model and Goland and Reissner's solution. The plots represent the adhesive stresses along the top adhesive/adherend interface from the center of the adhesive (x= 3.5) to the edges (x= 3,4).

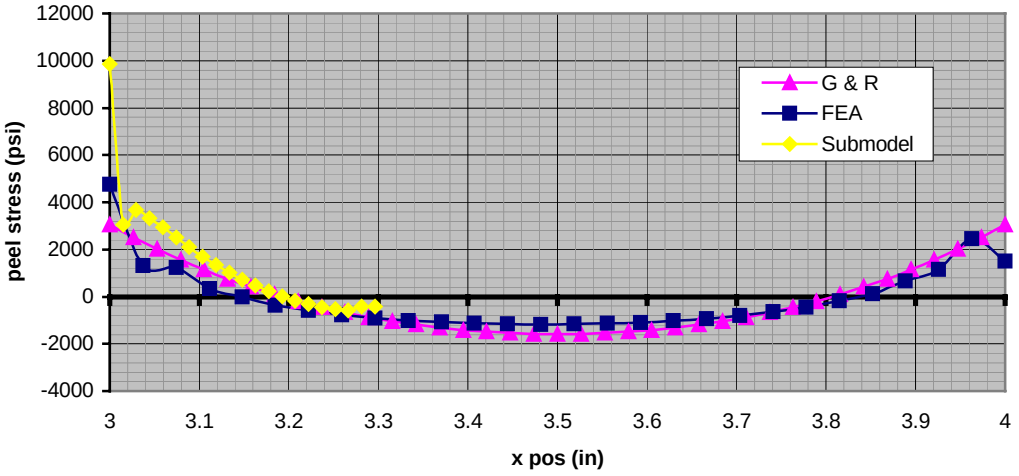


***Figure 3.4: Peel stress distribution in adhesive layer***

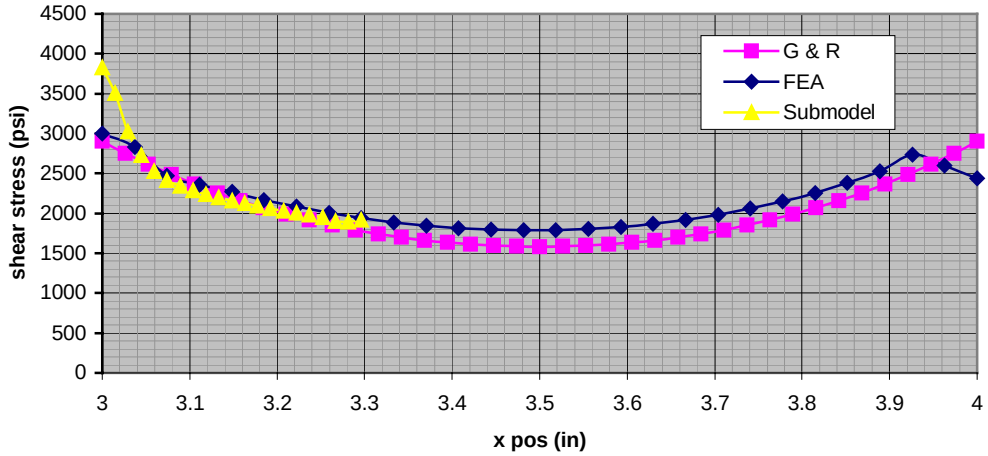


***Figure 3.5: Shear stress distribution in adhesive layer***

Note that the stress behavior is not symmetric along the upper interface in figures 3.4 and 3.5 for the FEA cases. This is due to the fact that differential shearing, as described by Volkersen in section 3.1, is more pronounced near the loaded edge. This edge corresponds to the side from which the adherend extends. Along the bottom interface of the adhesive, the stress behavior is switched so that the right side of the

interface is where the stresses are at a maximum. Goland and Reissner did not take into account these different edge effects in their formulation of peel and shear stresses. That is why their theoretical stress distribution is symmetric.

The sub-model analysis reveals that the stresses at the loaded edge increase dramatically as compared to the larger FEA model. In theory, shear stresses at a free surface are zero. Thus at the edge of the adhesive, which is a free surface, the shear stresses should go to zero. However, due to differential shearing, the shear stresses in the adhesive experience a maximum near the edges. Also, transverse normal, or peel stresses tend toward infinity at the edges. Due to this, the stresses are forced to decrease dramatically over a very small distance causing a stress singularity. One way to overcome this singularity is to use an extremely fine mesh in this area. However, the amount of computer processing time available for this analysis is limited which limits the degree of mesh refinement in the model. Because the mesh is not adequately refined, the elements used in this FEA cannot handle such an extreme stress gradient. Thus the edge stresses do not satisfy the boundary conditions. However the general trend of the stresses matched well with theory and was found to be satisfactory for this analysis. However, a large amount of computing time was necessary to solve the problem. Thus a simpler model was desired that was accurate yet more time efficient.

### 3.3.2 FEA Elastic Solution: Plane Model

The results of the solid model revealed that the stresses do not vary across the width of the joint. A three dimensional solution was not completely necessary. Therefore a two-dimensional plane element model was created to try and capture the

accuracy of a solid model without the large computer processing time. The plane model was solved at two different extremes, plane stress and plane strain. The geometry, material properties, boundary and loading conditions were kept the same as in the solid model. As seen in figures 3.6 and 3.7, the stress distributions matched very closely with the theory of Goland and Reissner. This close agreement was attributed to the similar assumptions made by both methods. As stated with the solid model, Goland and Reissner did not take the edge effects into account. Therefore the edge stresses experience a different trend in the FEA model than in the theory.

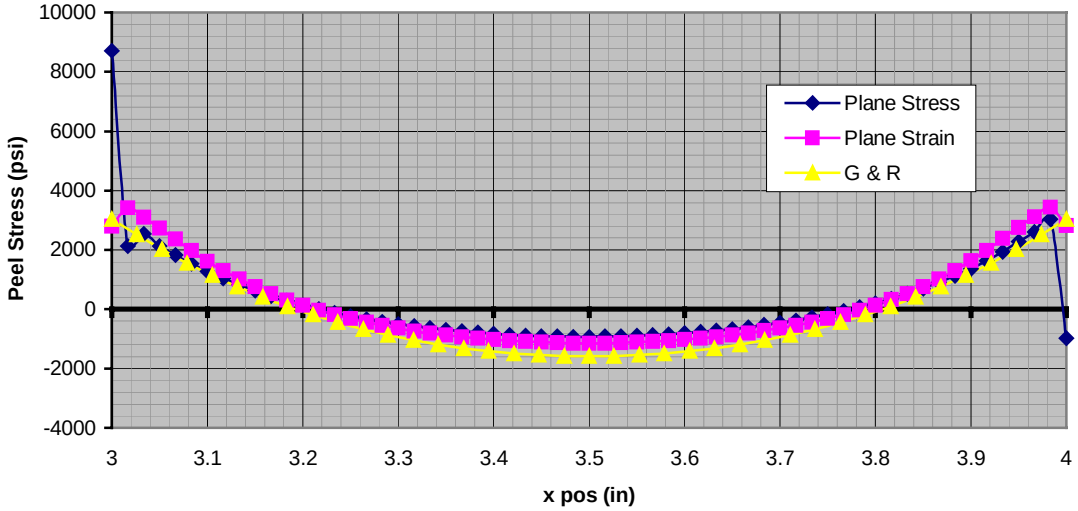


***Figure 3.6: Peel stress distribution in the adhesive layer***

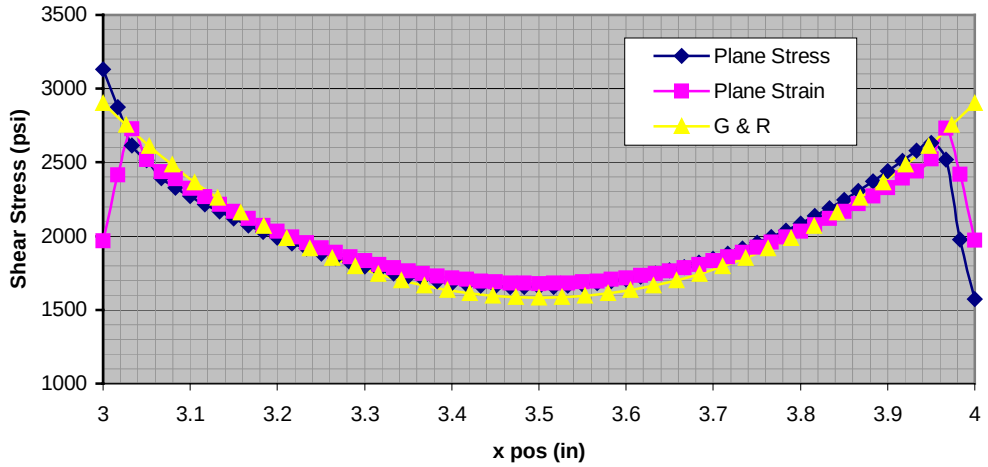


***Figure 3.7: Shear stress distribution in the adhesive layer***

While the three finite element models matched well with the classic solutions of Goland and Reissner, they were not capturing the actual behavior of the joint. Plasticity in the adhesive needed to be taken into account.

# 4. Elastic- Plastic Analysis of a Single Lap Joint

## 4.1 L. J. Hart-Smith

In an elastic analysis of the adhesive joints, the stresses in the adhesive are assumed to remain in the elastic region. However, the majority of modern adhesives have a large strain to failure. Once the yield stress is reached, the adhesive material properties become non-linear. This nonlinear behavior affects the actual stress distribution, raising the need for an elastic- plastic analysis. Also, because adhesives are so strong, the adherends may plastically deform before the adhesive fails. Thus adherend plasticity needs to be taken into account as well.

Using a continuum mechanics approach, L.J. Hart-Smith [4] developed an elastic-plastic analysis that characterized joint behavior into three failure modes. These modes include laminate- induced failures, adhesive shear failures, and adhesive peel induced failures. His design philosophy stated that the joint should never be the weak link. Details of the latter two modes of failure are described below.

When two adherends are bonded together and a load is applied to the ends, differential movement of the adherends creates stresses and strains in the adhesive. Recall from Volkersen's analysis that the tensile stress and strain in the adherend is at a maximum at the edge of the bond line from which the adherend extends. Thus the movement in the adherend is not constant. Therefore the adhesive shear strain is non-uniform across the bond line. Different sources of this shear strain need to be accounted

for. According to Hart-Smith, there are three major sources of this [7]. The first source is the strain concentration due to adherend extensibility.

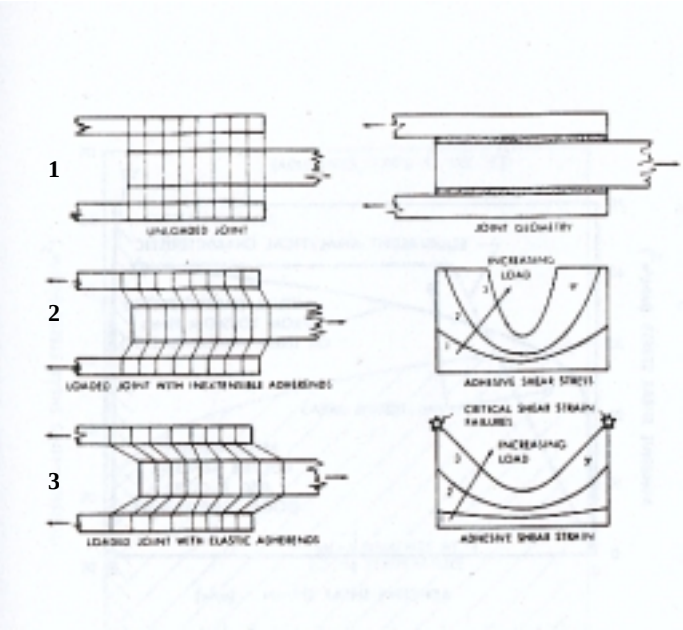


***Figure 4.1: Adhesive shear stress and shear strain for stiff and elastic adherends [4]***

As seen in figure 4.1, the shear stresses and strains peak at the edges of the overlap and then decrease towards the middle. Stiffer adherends experience less of a differential shear strain distribution as well as a less intense strain concentration, making them more efficient.

The second source arises from an adherend stiffness imbalance. Within the adhesive, the shear strains are more intense at the end from which the softer adherend extends. The less critical end, that being the one from which the stiffer adherend extends, is unloaded, shifting the effective area of the adhesive to the critical end. This, in turn, reduces the overall joint strength.

The third source of non-uniform shear strain occurs when the adherends have different coefficients of thermal expansion. Typically, an adhesive is cured at temperatures much greater than the operating temperature. As the temperature cools, the adherend with the higher coefficient will tend to shrink more than the adherend with a lower coefficient. This creates residual bond stresses at the edges.

The load is transferred through the adhesive by two end zones with a lightly loaded elastic trough in-between as seen in figure 4.2.

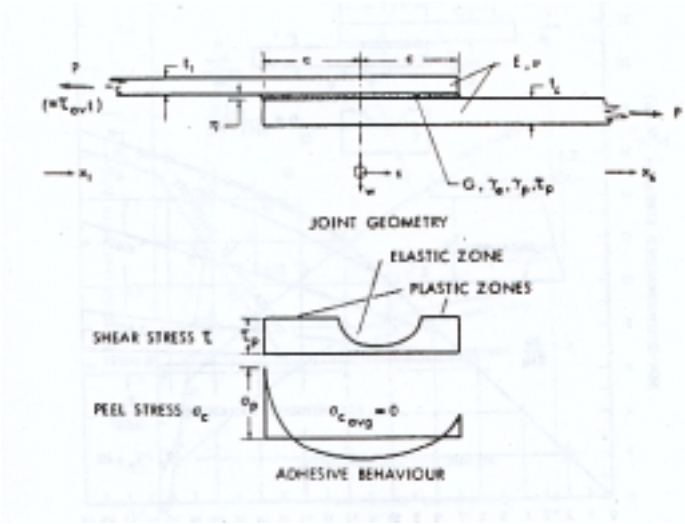


***Figure 4.2: Single Lap Joint Stress Distribution [4]***

The adhesive plasticity and not the length of the overlap define the lengths of theses end zones. With the exception of very short overlaps, increasing the overlap length simply moves these plastic zones further apart. The maximum stresses and strains are not affected.

In addition to the shear stresses, peel stresses are developed in the adhesive and experience a maximum at the edges. As the applied load increases, these stresses pull on the laminate fibers causing them to split apart locally. Once the laminate splits, no shear transfer can occur between the inner and outer plies of the composite. The outer fibers then become overloaded and break in tension. Figure 4.3 illustrates this failure mode. The presence of peel stresses limits the thickness of the adherends that can be bonded together efficiently.

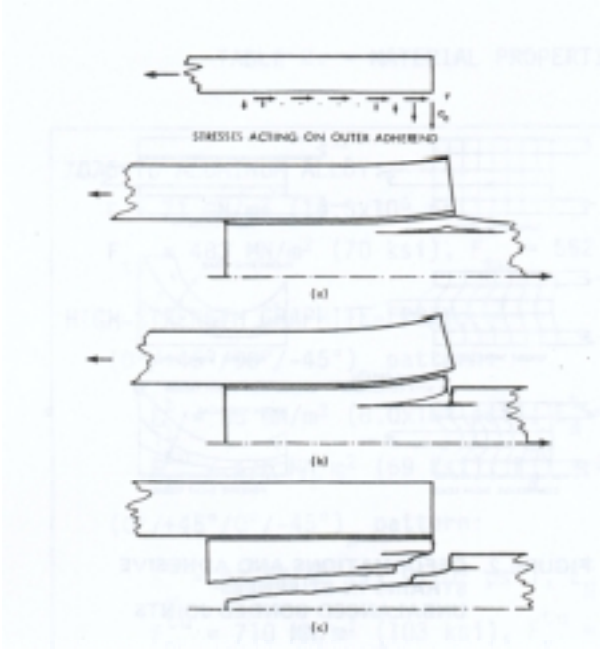


***Figure 4.3: Peel Stress Failure Mode in Composite Joints [4]***

Taking into account all of these failure modes, an accurate model for the adhesive was developed. Hart-Smith idealized the adhesive stress-strain relationship as elastic-perfectly plastic. This stress strain curve is illustrated in figure 4.4.

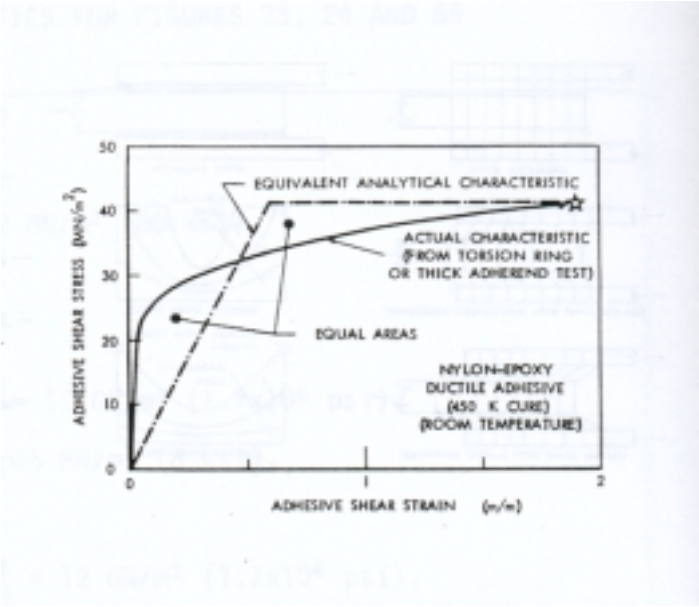


***Figure 4.4: Hart-Smith's Elastic Plastic Stress-Strain Curve [4]***

By setting the adhesive failure stress equal to the yield stress, failure is assumed to occur when the adhesive reaches its limiting shear strain.

As compared to the elastic solutions, Hart-Smith's theory matched very well with experimental data. It was therefore decided that adhesive plasticity needed to be added to the FEA models in order to make them as accurate as possible.

## 4.2 FEA- Elastic Plastic Analysis

The plastic behavior of the adhesive was incorporated into the plane42 element models under plane stress and plane strain. Due to computer processing time constraints, a solid model of the elastic- plastic model could not be solved for. Plasticity in the adherends was not taken into account due to the lack of yielding under loading. Unlike a typical metal that experiences some yielding before fracture, the composite fails soon after the yield stress is reached. The stress strain curve of the adherend was therefore assumed to remain linear.

Uniaxial tensile tests performed by Ashland Chemical on the PLIOGRIP Structural Adhesive indicated that the stress-strain behavior becomes non-linear once the yield stress is reached. Plastic hardening was not included in the analysis. Rather the adhesive behavior was modeled as elastic perfectly plastic (EPP). Insuring that the area under the actual stress-strain curve was the same as the area under the approximated curve made a good approximation of the EPP stress strain curve. The yield stress was set at 2250 psi. Figure 4.5 shows the two stress strain curves.

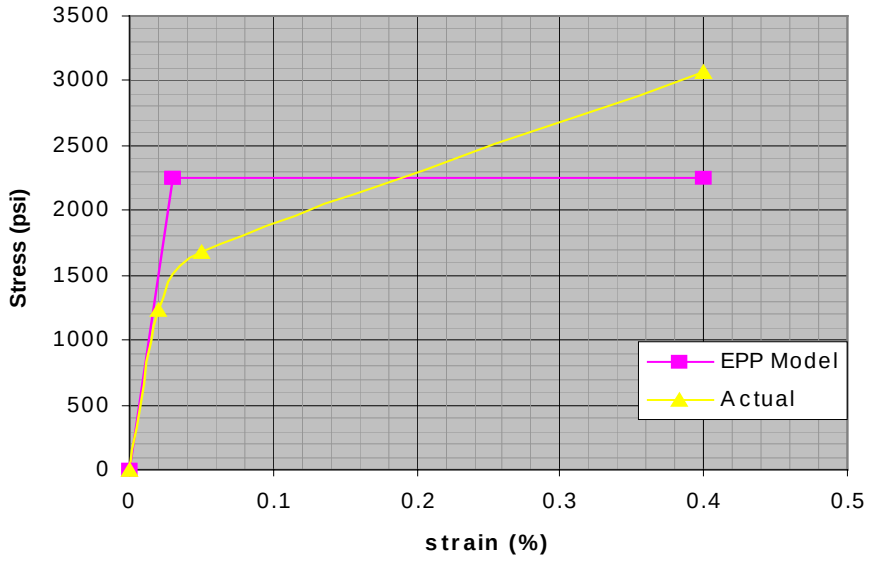

***Figure 4.5: Adhesive Stress-Strain Curve***

### 4.2.2 Simple Beam Problem

Before a plastic analysis on a single lap joint was conducted, two simple models were built where the answer could easily be solved for analytically. This was necessary in order to gain confidence in the methodology of the plastic analysis.

The first problem involved a rectangular beam under axial loading shown in figure 4.6.

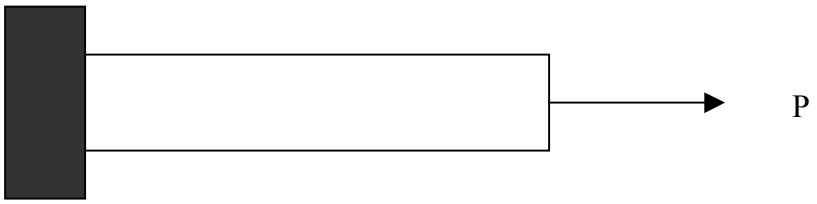


***Figure 4.6: Beam in axial loading***

The beam was modeled as elastic perfectly plastic with a yield stress of 300 MPa and a Young's Modulus of 200 GPa. The beam had a length of 500mm, a width of 20mm and a height of 30mm.

Using equations (4.1) through (4.3), the strain and deflection were calculated in the elastic region and a stress-strain curve was generated. Once the stress equaled the yield stress of the beam, the stress-strain slope was zero due to the elastic-perfectly plastic assumption. Then, the problem was solved on ANSYS using Plane42 elements.

$$\delta = \frac{FL}{EA} \qquad (4.1)$$

$$\varepsilon = \frac{\sigma}{E} \qquad (4.2)$$

$$\sigma = \frac{F}{A} \qquad (4.3)$$

As seen in figure 4.7, the results between the analytical and numerical method were identical.

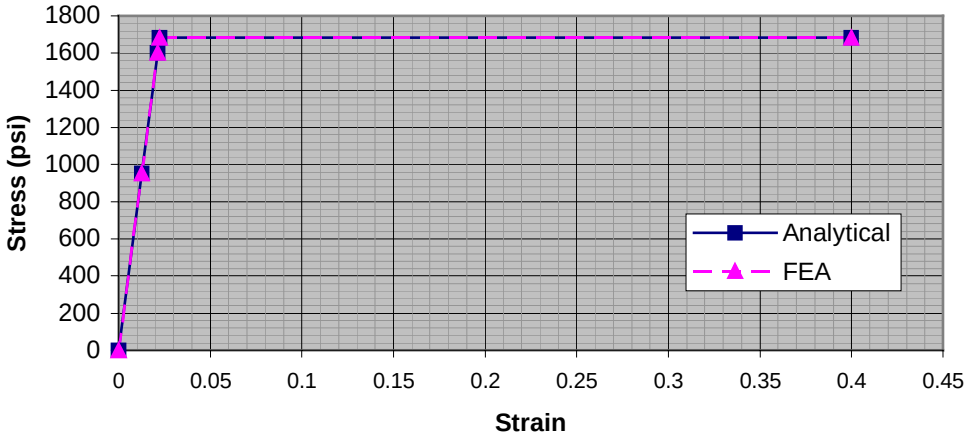


***Figure 4.7: Stress Strain curve for beam under axial loading***

The second problem consisted of a beam in bending as shown in figure 4.8.

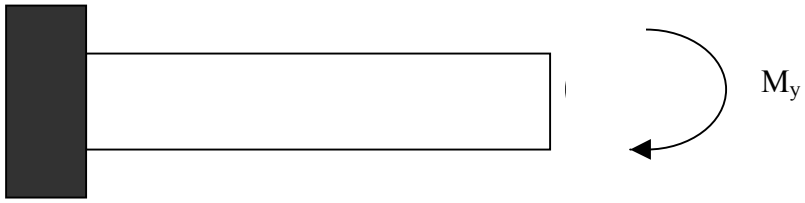


***Figure 4.8: Beam in bending***

The beam cross-section was 1.0 inch wide by 1.0 inch thick with a length of 48 inches. The yield stress was 1683 psi. In the elastic region, the stress is given as:

$$\sigma = \frac{Mc}{I} \tag{4.4}$$

Where $M$ is the bending moment, $c$ is half the thickness and $I$ is the moment of inertia. When the yield stress, $S_y$ is reached, the bending moment is given as:

$$M_y = \frac{2}{3} bc^2 S_y \tag{4.5}$$

Where

$$I = \frac{1}{12} b(2c)^3 \tag{4.6}$$

In equations (4.5) and (4.6), $b$ is the width of the beam. This yielding moment was calculated as 280.5 inch-lbs. At this point, the beam becomes partially plastic. As the moment is increased, the plastic zone increases. Using ANSYS, the beam was loaded with three different moments to verify the transition from elastic to partially plastic behavior. Figure 4.9 shows the results of the numerical analysis which were as expected.

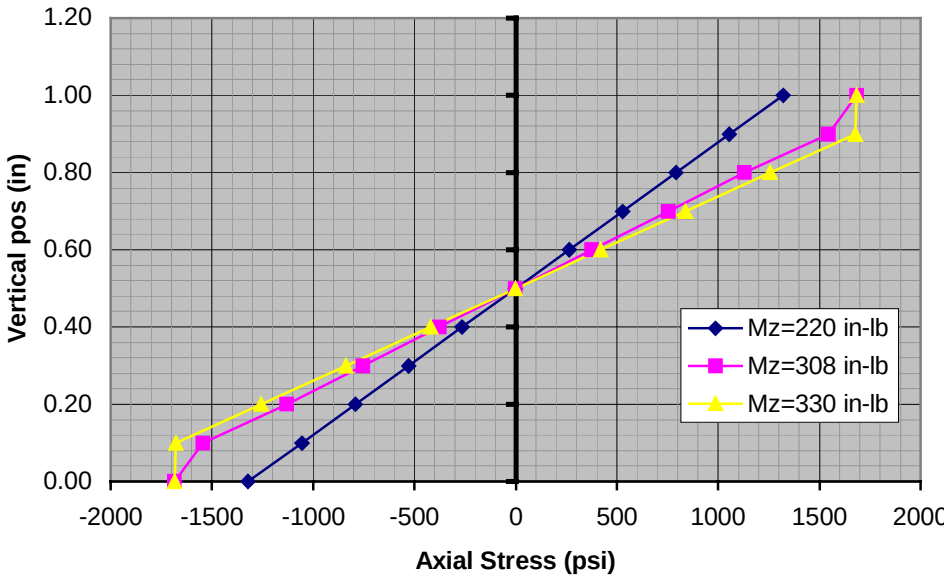


***Figure 4.9: Increasing plastic zone in axial stress for a beam in bending***

Note that as the moment is increased, the slope of the line changes at the top and bottom of the beam. This indicates that the plastic zone in the beam is increasing due to plastic yielding of the material. Once the simple problems were verified, the elastic-plastic analysis of the single lap joint was continued.

### 4.2.3 Plane Stress and Plane Strain

Using the same joint configuration as in the elastic case, an elastic-perfectly plastic analysis was carried out for both plane stress and plane strain. Nonlinear geometry was taken into account due to the bending moments arising from the eccentricity of the load path. Using 17 load steps, a maximum static load of 2000 lbs was applied to the joint. The shear and peel stress distributions are shown in figure 4.10 and 4.11.

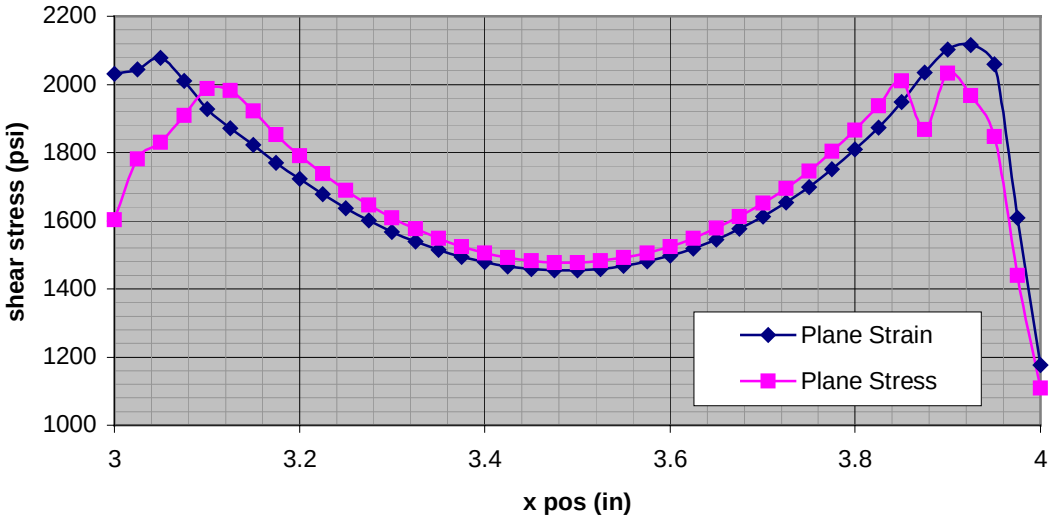


*Figure 4.10: Shear stress distribution in Plane42 Elastic-Plastic FEA*

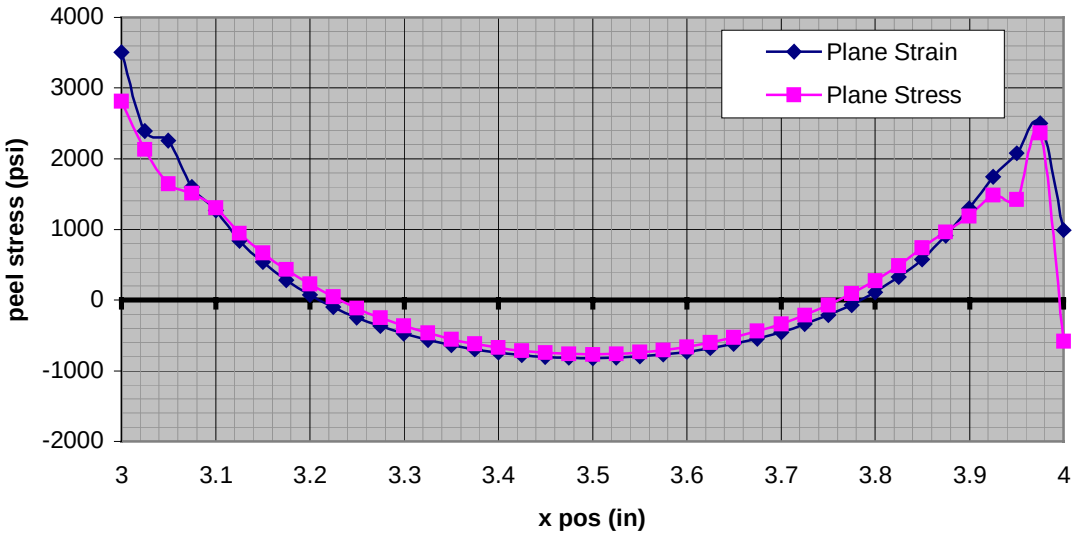


*Figure 4.11: Peel stress distribution in Plane42 Elastic-Plastic FEA*

The overall behavior of the stress distribution matches closely with that of Hart-Smith's theory (see figure 4.2). Looking at figure 4.10, the edges tend to flatten out due to adhesive yielding. The maximum shear stress in the elastic-plastic model is about 2100 psi. In the elastic model, the maximum is about 2700 psi. Figures 4.12 and 4.13

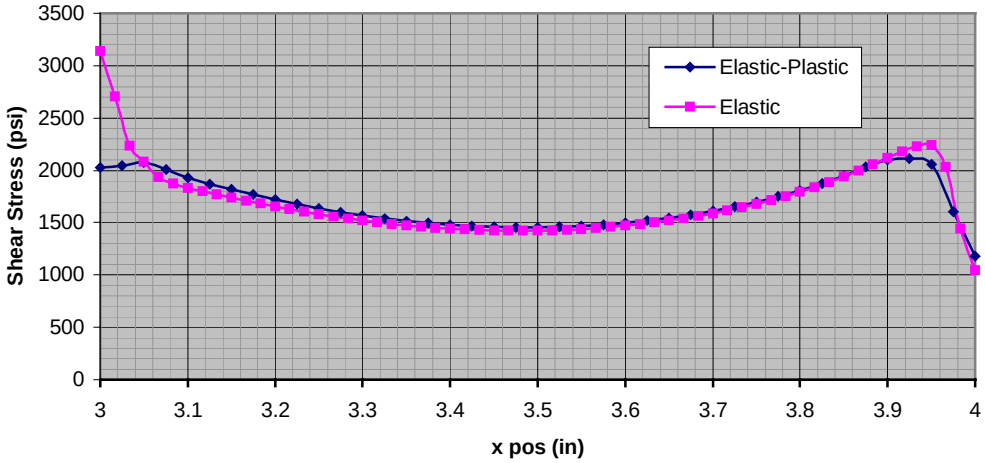


show the difference between the shear and peel stresses for the elastic and elastic-plastic cases.

***Figure 4.12: Comparison of shear stress distributions for elastic and elastic-perfectly plastic cases***

***Figure 4.13: Comparison of peel stress distributions for elastic and elastic-perfectly plastic cases***

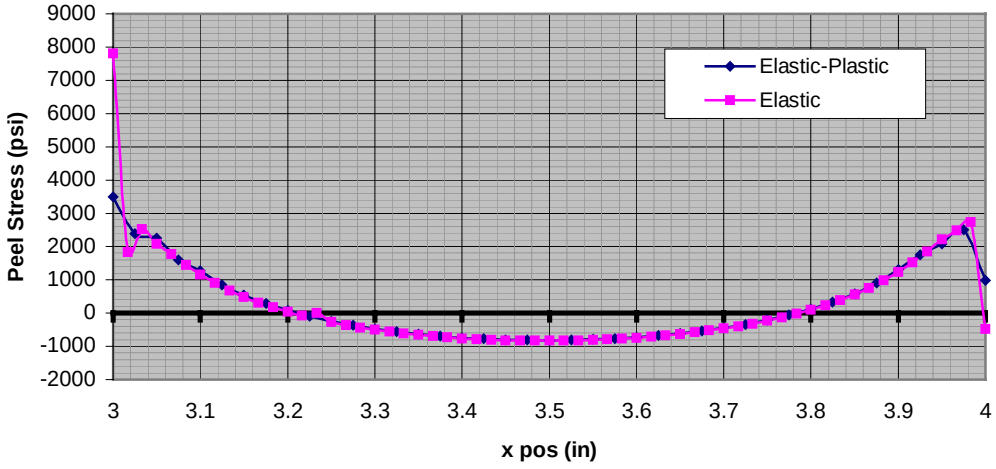

The dramatic drop in magnitude is due to the plastic behavior in the adhesive. Note the adhesive yielding at the edges in the elastic-plastic curves.

In order to carry out the parametric study on different joint configurations, one model had to be chosen. In a typical joint, the width is large compared to the thickness. Therefore the elastic-plastic two-dimensional plane strain model was implemented for the remainder of this study.

# 5. Parametric Study

Using finite element analysis, a parametric study was carried out on a single lap joint. The goal was to alter the geometry and material properties of the joint and study their effects on the stress distribution of both the adherends and adhesive. Four different cases were studied. The first involved adding a taper to the edges of the adherends. The second case involved changing the adhesive edge shape. The edge shapes investigated were square, convex and concave. The third case involved changing the material properties in order to create a material stiffness imbalance. In the final case, the thickness of one adherend was altered to create a geometric stiffness imbalance.

## 5.1 Failure Criteria

A failure criterion was established in order to have a baseline for comparison between the different parametric cases. Failure in a single lap joint can occur either in the adhesive layer or the adherend. Because of this, two different criteria were used to track both adhesive and adherend failure.

### 5.1.1 Adhesive Failure

It is generally accepted that yielding in adhesives depends on both the hydrostatic and deviatoric stress components. A hydrostatic stress state occurs when all three principal stresses are equal. In this condition, the normal strains are equal, the shear stresses are zero and the stressed element experiences no distortion. Once this stress state is altered, distortion will occur. The stresses that cause distortion are termed the

deviatoric stresses. The von Mises yield criterion takes these two components into account in the derivation of an equivalent von Mises stress defined as:

$$\sigma_{\text{von Mises}} = \sqrt{0.5*[(\sigma_1-\sigma_2)^2+(\sigma_2-\sigma_3)^2+(\sigma_3-\sigma_1)^2]} \qquad (5.1.1)$$

Yielding occurs when the following condition is met:

$$\sigma_{\text{von Mises}} = S_y \qquad (5.1.2)$$

Where $S_y$ is the yield strength of the material and $\sigma_1$, $\sigma_2$, $\sigma_3$, represents the three principal stresses.

Because the adhesive is modeled as elastic-perfectly plastic, the von Mises stress can reach the yield stress without the adhesive failing. That is because it has not yet reached its limiting shear strain value. By tracking the von Mises stress as well as the shear strain on the finite element models, a good approximation for failure in the adhesive can be made. The limiting shear strain of PLYOGRIP structural adhesive was about 40% in experimental tests.

### 5.1.2 Adherend Failure

Debate still continues over a suitable failure criterion for composite materials. Unlike metals, a criterion that would consistently and accurately predict failure has yet to be determined. Factors such as misaligned fibers during manufacturing and voids in the matrix can adversely affect the strength of the composite from one specimen to the next making it difficult to predict failure. However, some baseline for comparison of the parametric cases needed to be established. As described by Hart-Smith, failure in a single lap joint can occur due to a high peel stress concentration in the adhesive at the edge of the overlap. The result of these peel stresses is a crack in the composite adherend

that propagates through the thickness of the laminate. Once this crack starts, delamination in the laminate occurs. Tests performed at North Carolina State University showed this type of failure consistently for fiber tear failure modes. A failed specimen is shown in figure 5.1.

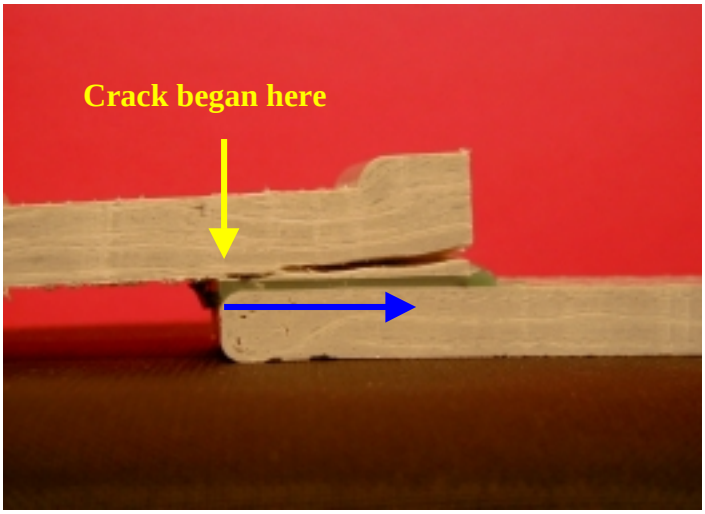


***Figure 5.1: Typical Failure in a composite single lap joint***

The origin of the crack in the laminate began at the critical area of the upper adherend as indicated by the yellow arrow. The crack then propagated across the bond line as indicated by the blue arrow. However, the crack did not follow a straight-line path across the interface of the bond line. Rather, it tore through the layers in the laminate causing interlaminar failure. Looking at figure 5.1, the crack penetrated through at least one layer in the composite. An interlaminar failure criterion was therefore needed to help predict the failure of the composite.

The most basic interlaminar failure criterion is that of maximum stress. This criterion assumes that interlaminar failure occurs when the normal tensile stress at the interface exceeds its ultimate strength, e.g.

$$\frac{\sigma_z}{Z} = 1 \tag{5.1.3}$$

Where $Z$ is the interlaminar tensile strength of the adherends and $\sigma_z$ is the peel stress at the interface. However, this is not a sufficient criterion because it does not take into account the effect of shear and longitudinal stresses in delamination. One criterion that takes into account the interaction of these additional stresses is the Tsai criterion, which is given as:

$$\frac{\sigma_x^{\,2} - \sigma_x \sigma_z}{X_T^{\,2}} + \frac{\sigma_z^{\,2}}{Z^2} + \frac{\tau_{xz}^{\,2}}{R^2} = 1 \tag{5.1.4}$$

Where $X_t$ is the ultimate tensile strength in the laminate and $\sigma_x$ is the longitudinal stress in the surface ply. $R$ is the through-the-thickness shear strength of the composite and $\tau_{xz}$ is the shear stress at the interface. This theory was used as a point based criteria. That is, the values for the stresses were taken at a node where they were at a maximum. These nodes were consistently located at the edges of the bonded area. This area is outlined in figure 5.3. The Tsai criterion was used to establish an approximate load where the joint may fail. However, for the parametric cases, it was advantageous to look at the stress gradients as well to better understand the effects the parameters had on the joint.

Table 5.1 lists the longitudinal and shear strengths of the composite. Values were taken from tests performed at Delsen Testing Laboratories on MMC composite panels.

**Table 5.1 Material strengths of MMC composite**

| Direction | Strength (psi) |
|---|---|
| $X_t$ | 9390 |
| Z | 9390 |
| R | 2520 |

## 5.2 Adding a taper

As explained earlier, adhesive peel stress is one of the critical stresses that can cause failure of a joint. In the case of double lap joints, reducing the peel stress in the adhesive can significantly improve the overall strength of a joint. It was desired to investigate the effects adding a taper would have on a single lap joint.

The cases studies involved a 90˚, 45˚ and 30˚ taper. The taper was created at the unloaded end of each composite. Note that the angle is measured from the horizontal plane. Figure 5.2 shows the different taper angles.

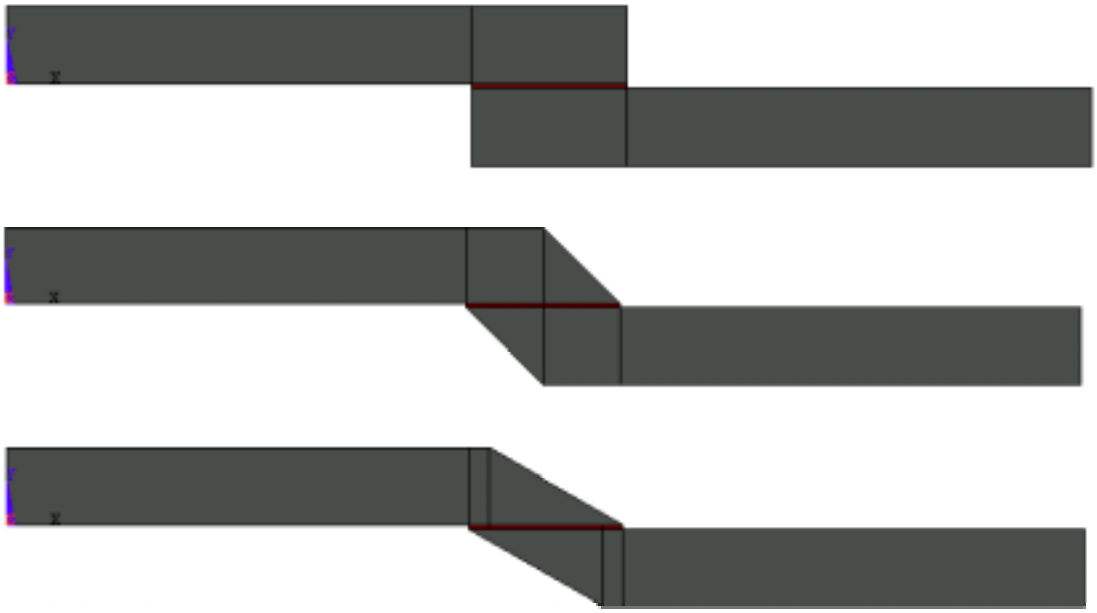

***Figure 5.2: 90, 45 and 30 degree taper angles for the single lap joint***

The critical areas of a single lap joint are at the corners of the bond line along the adherend/adhesive interface from which the adherend extends. The opposite corner is referred to as the less critical end. At the critical areas, differential shearing is more pronounced, creating a more severe stress state in the adhesive. In addition, the majority of load is transferred from one adherend to the other at these regions. This concept is shown in a vector plot of the principal stresses for a 90º taper joint in figure 5.3. In this plot, the arrows indicate the direction of the stress, and their size represents the stress magnitude. The black, blue and yellow arrows represent the first, second and third principal stress, respectively. Note the high density of arrows in the critical areas in the joint as compared to the less critical areas.

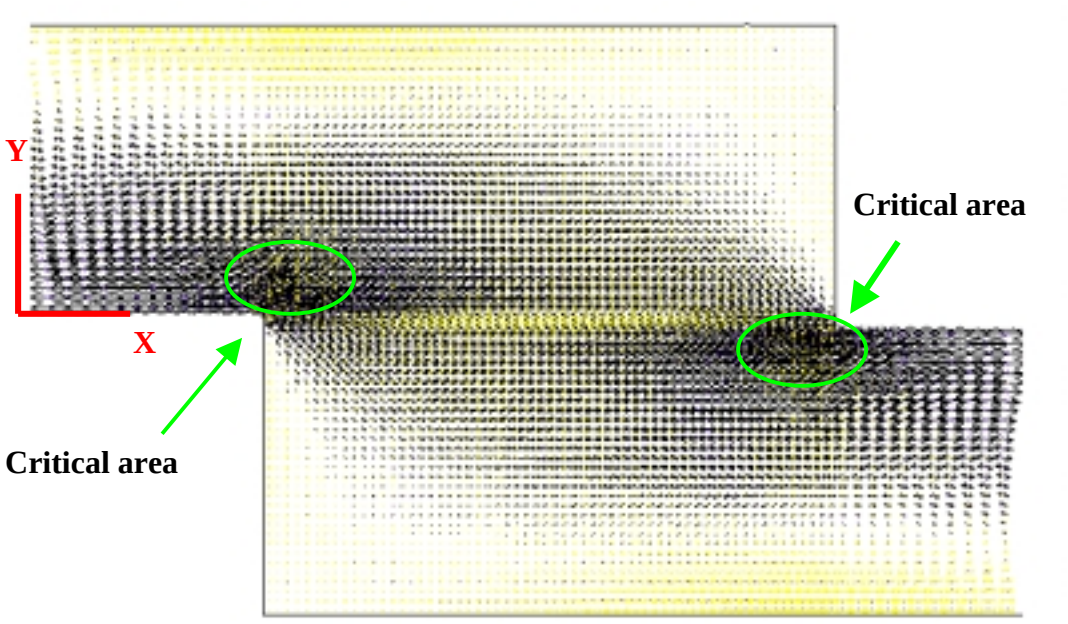


***Figure 5.3: Principal Stress Distribution in a Single Lap Joint***

Figure 5.4 shows the peel stress distribution in the adhesive along the upper adherend/adhesive interface. The center of the adhesive layer is at x=3.5. While the peel stress in the adhesive layer at the less critical end is decreased with an added taper, the critical end is not affected. It was also found that adding a taper did not affect the shear stresses in the adhesive.

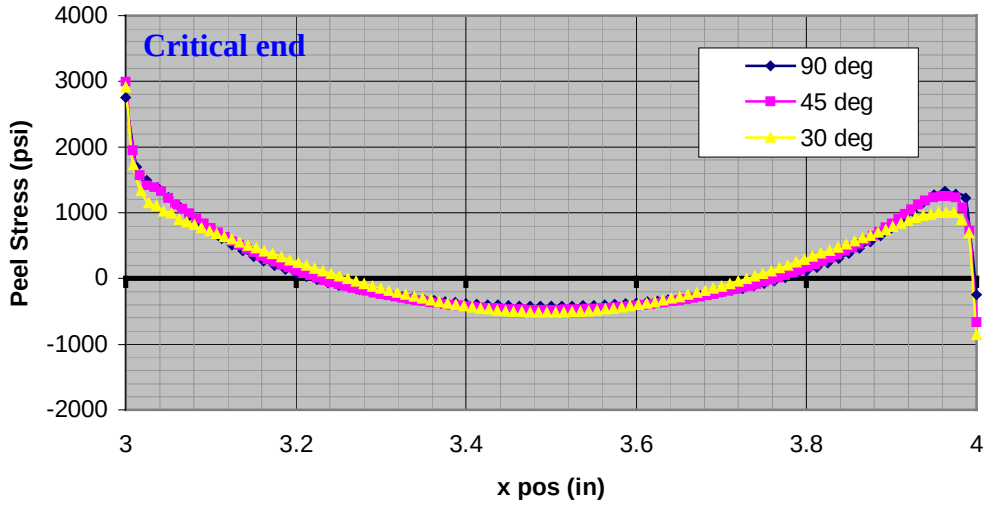


***Figure 5.4: Peel Stress Distribution for Increasing Taper***

In a 90˚-tapered joint, the adherend satisfies the Tsai failure criteria at an applied load of 950 lbs. The adhesive experiences some yielding at the critical corners but the maximum shear stress is only 8%. Therefore, the adherend is assumed to fail first. In both the 45˚ and 30˚-tapered joints, the failure criterion is satisfied at 1000 lbs of load. The adhesive experiences some yielding but the maximum shear strain is still only about 8%. Again, the critical regions are in the adherends. The 5% increase in the maximum load before failure for the tapered joints is due mainly to a decrease in peel stress in the adherends. While this decrease is a positive trend, there is a significant increase in axial stress in this same area. This axial stress coincides with the first principal stress of the joint. This increase was due in part to the stress concentrations built up in the corner of the adherend with the taper. As the taper is increased, the area of load transfer from one adherend to the other is reduced while the amount of load that needs to be transferred

remains the same. Figure 5.5 shows the progression of this stress concentration in the lower adherend and the effect it has on the upper adherend. Note that the adhesive layer is not included in the figures. For each case, the applied load was 950 lbs. The scale at the lower left hand side of each case is the first principal stress range in units of psi.

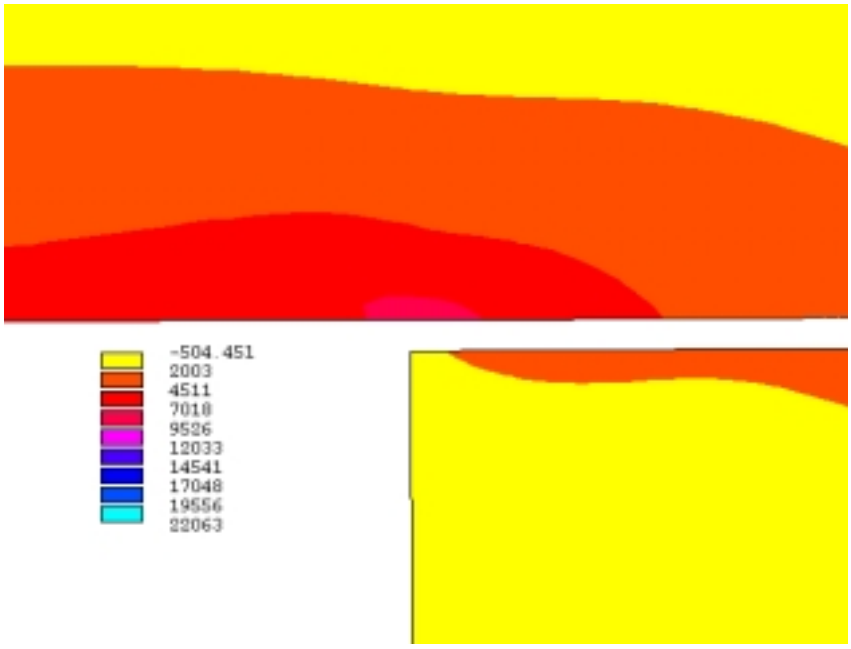


(a) 90˚ taper

***Figure 5.5: First Principal Stress Distribution with Varying Degree of Taper***

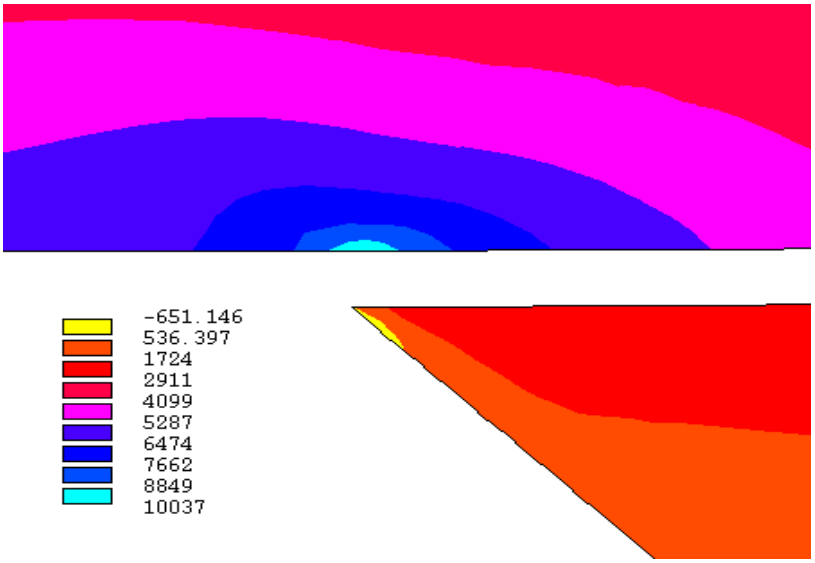


(b) 45˚ taper

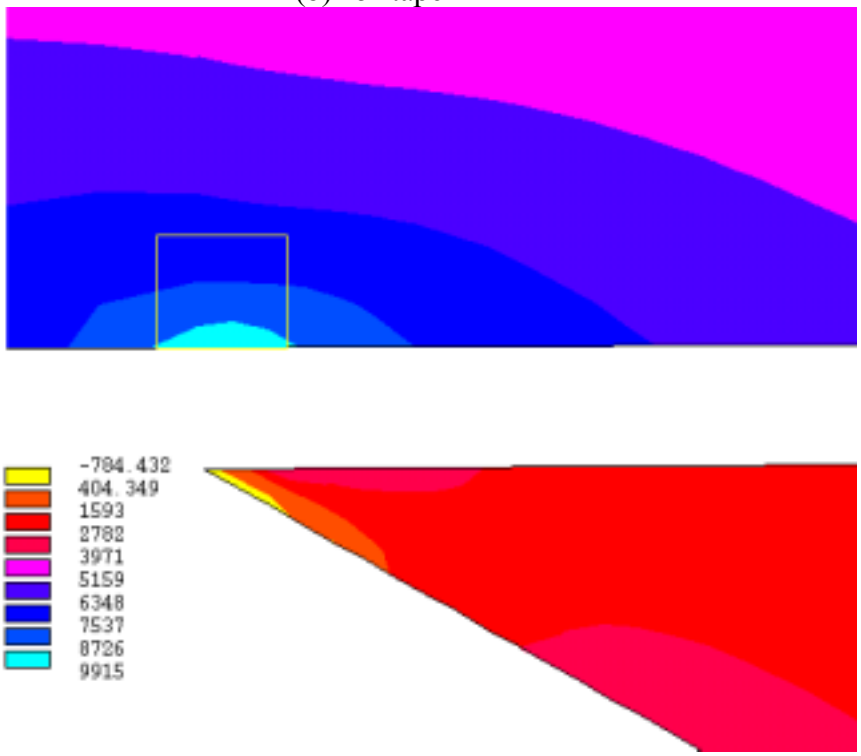


(c) 30˚ taper

***Figure 5.5 (continued)***

In addition to a stress increase in the lower adherend, there is a stress increase in the upper adherend at the critical area. As the taper is increased, the magnitude of stress in the critical area is increased. In order to illustrate this point, figure 5.6 shows the stress gradient of each tapered joint within an area equal to the square of the adhesive thickness around the critical area. This area is outlined in yellow on figure 5.5(c).

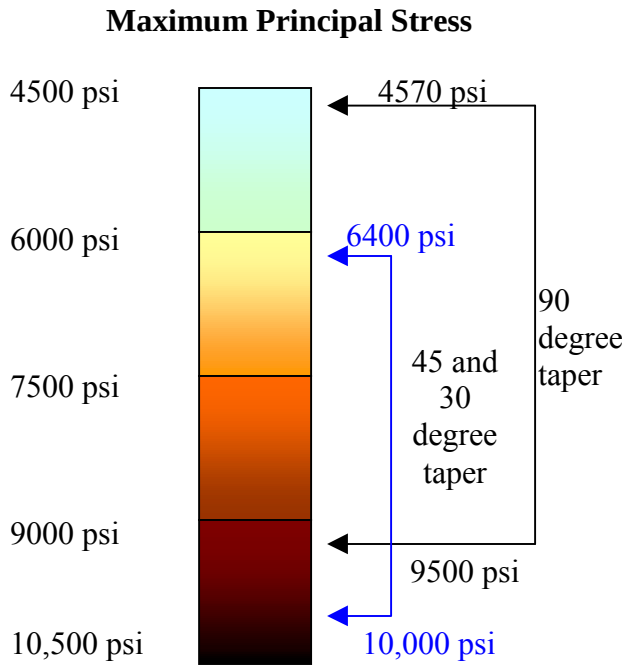


***Figure 5.6: First principal stress gradient for tapered joints***

Figure 5.7 depicts the percentage of high stress within the given area for the 45 and 30 degree taper. Thus the amount of high stress is increased within the given area with an increase in taper.

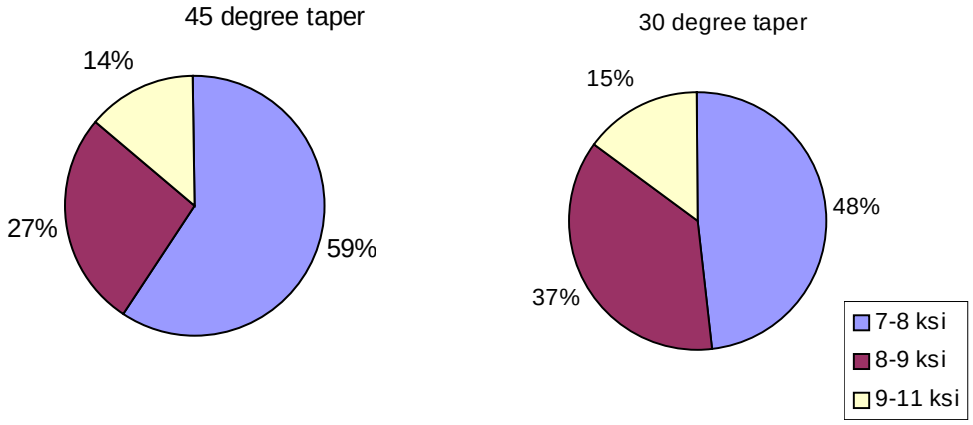


***Figure 5.7: Percent of stress in adherend for a 45 and 30 degree taper***

Note that for the 45 degree taper, 14% of the stress is between 9-11 ksi and 27% is between 8-9 ksi. By increasing the taper to 30 degrees, the 9-11 ksi stress range increases to 15% and the 8-9 ksi increases to 37%.

In conclusion, while a taper can increase the bond strength of a double lap joint, it creates a more severe stress state in the single lap joint. This may adversely affect the overall behavior of the joint.

## 5.3 Different Edge Shapes

For all of the finite element models, the edges of the adhesive were modeled as square. In reality, when the joint is made, extra adhesive is squeezed out the sides forming a rounded fillet at the ends. Studies carried out by Adams and Peppiatt revealed that these fillets could reduce the stresses at the edges by up to 30% [1]. This reduction in stress gives a stronger bond and, in turn, a higher load to failure. The types of fillets studied by Adams et al were triangular in shape. It was desired to study the effects of different edge shapes on the adhesive, namely a square, convex and concave shape. As

explained earlier, a convex shape occurs due to extra adhesive being squeezed out the sides of the joint. If that extra adhesive is wiped off, a concave fillet is created. The convex and concave fillets were formed with a radius equal to the adhesive thickness. Figure 5.8 shows the different edge shapes studied.

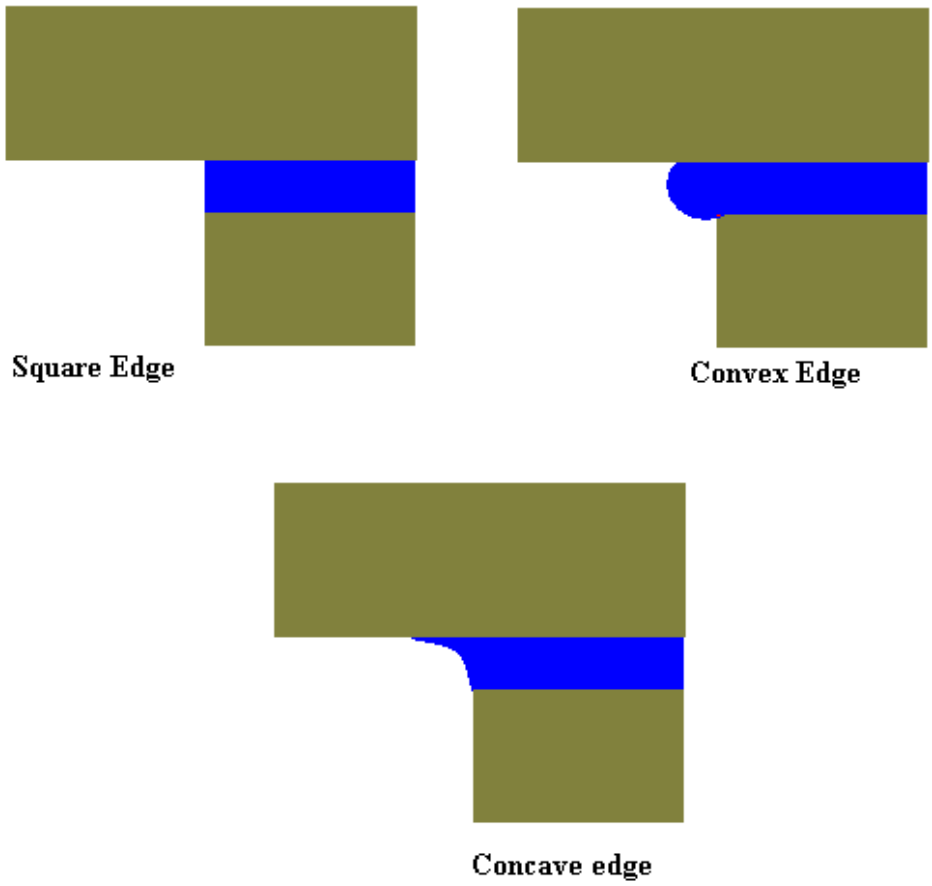


***Figure 5.8: Square, convex and concave edge shapes of adhesive***

The square and convex cases satisfied the Tsai failure criterion at 950 lbs while the concave case satisfied the criterion at 1000 lbs. As in the tapered case, this

information is not enough to fully understand what happens to the stress distribution in the joint. Figure 5.9 shows a vector plot of the principal stresses in the joint at the critical area.

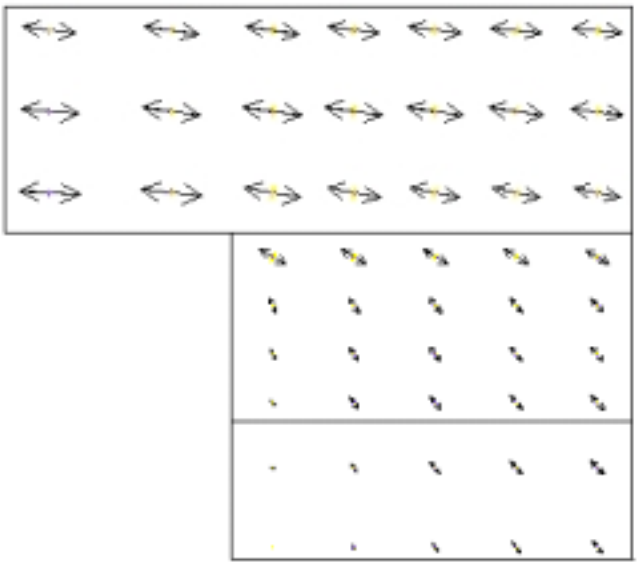

(a) Square edge

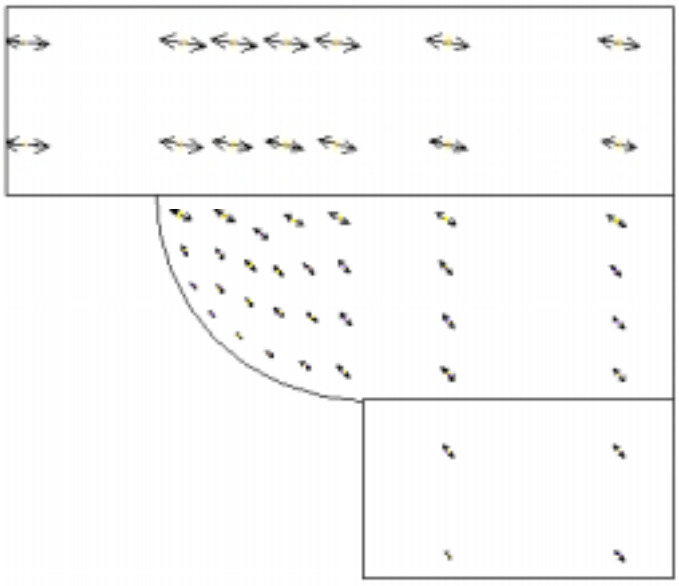

(b) Convex edge

***Figure 5.9: Principal Stress plot for (a) Square (b) Convex and (c) Concave edge shapes***

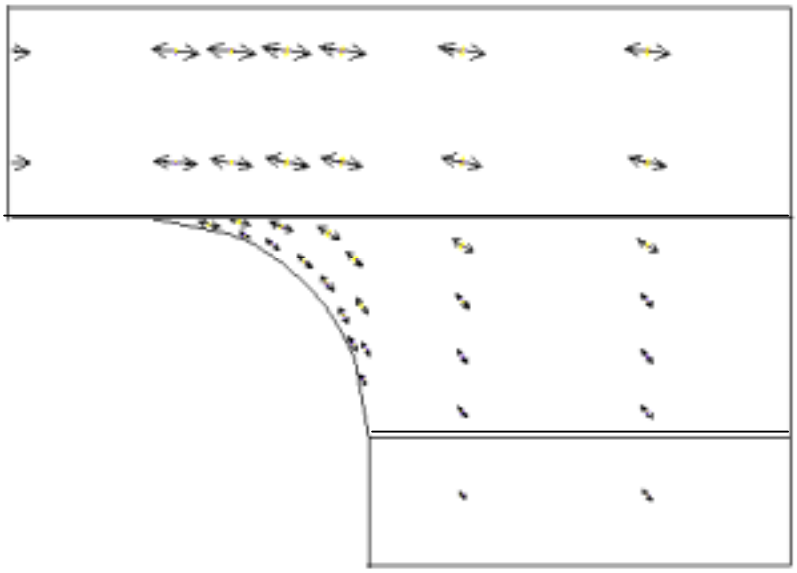

Concave edge

***Figure 5.9 (continued)***

If a specimen under loading has sharp edges, stress concentrations will occur there. As stated earlier, the majority of the load transferred from one adherend to the other is done so at the edges of the adhesive layer. In figure 5.9(a), the square edge acts as a stress riser, making it difficult for the load in the adhesive to transfer into the adherend. As a result, a stress concentration is built up in both the adhesive and adherend. The convex edge in figure 5.9(b) still produces a sharp edge for the load to transfer over, but the surface area is increased allowing for an easier diffusion of load from one adherend to the other. The concave fillet, shown in figure 5.9(c), shows the smoothest transition of load. With this fillet, the singularity is reduced. The effect these edge shapes have on the adherend is that the maximum principal stress in the critical area is decreased

slightly. In addition, the gradient of stress in this area is decreased. Using the same area as used in figure 5.6, a range of principal stresses is plotted in figure 5.10.

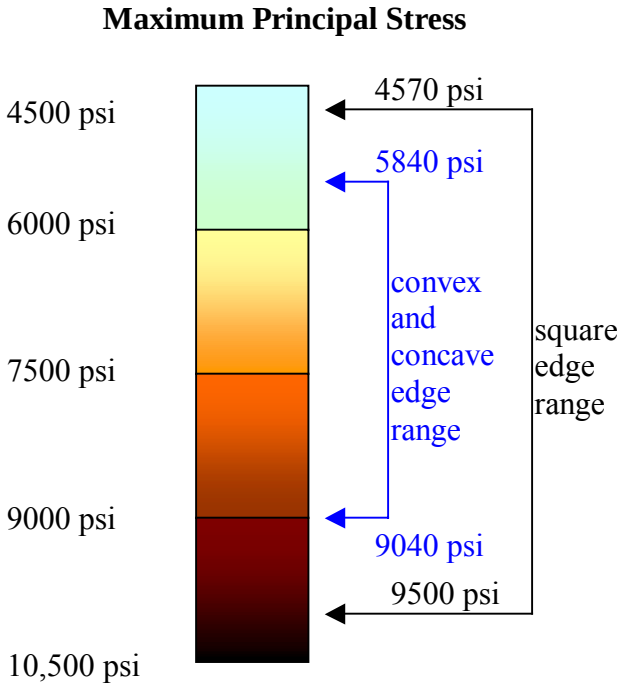


***Figure 5.10: Principal stress range in critical area of adherend***

Within the same area, the maximum principal stress gradient is reduced by a factor of 1.54.

With respect to the adhesive peel and shear stresses, the difference between the square and convex shape is minimal. However, there is a significant change with the concave shape. Figure 5.11 shows the peel stress distribution in the adhesive. The stress in the concave edge case is dramatically reduced and the trend is changed from increasing at the critical area to decreasing. This is due mainly to the fact that sharp corner is removed so the singularity is significantly reduced.

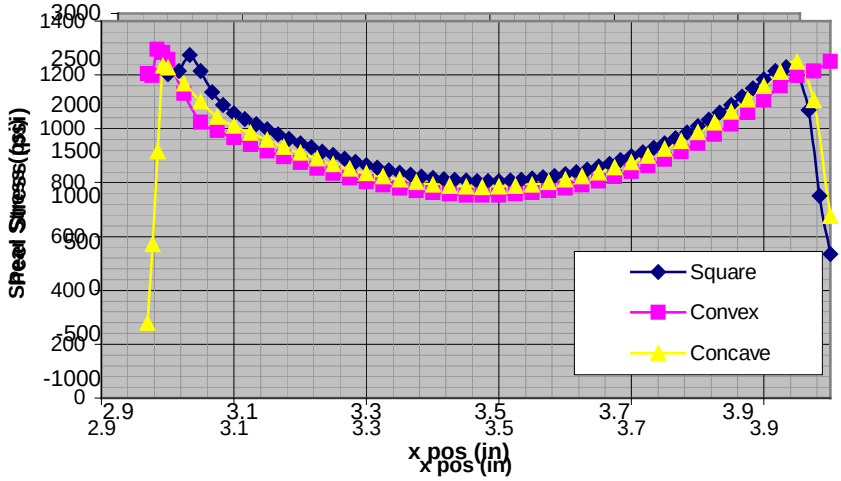


***Figure 5.11: Adhesive peel stress for different edge shapes***

Figure 5.12 shows the shear stress distribution in the adhesive. The maximum stress attained in the concave edge case at the critical side is about 8% lower than the square or convex edge cases. As discussed earlier, a stress singularity exists at the corner of a square edge. The concave fillet relaxes that singularity and the shear stress is reduced towards zero. In addition, because the shear stress is reduced, differential shearing at the edges is reduced as well. Therefore the adhesive does not experience any yielding at this load. The convex and square edge both experienced some yielding at the edges where the shear stress is at a maximum. The shear strain for these two cases was about 8%.

***Figure 5.12: Shear stress in adhesive for different edge shapes***

In conclusion, either a convex or concave fillet will slightly reduce the stress concentration that occurs at the edges of the bond line in the adherend. However, a

concave fillet will significantly reduce the shear and peel stresses in the adhesive layer at the edges. Therefore a concave fillet will yield the best overall joint behavior.

## 5.4 Stiffness Imbalance

The stiffness of a structure can be described as its ability to resist deformation. This stiffness depends on both the geometry and the material property of the structure. For example, the stiffness of a beam in axial loading is given by:

$$k = \frac{EA}{L} \qquad (5.1)$$

Where $E$ is the Young's Modulus, $A$ is the cross-sectional area and $L$ is the length. By changing either the geometry or the material property, the stiffness is altered.

The most efficient joint is a balanced joint. That is, the geometry and material properties of both adherends are identical. If an imbalance exists, the joint becomes weaker. A study was performed to investigate the effects of both a material stiffness imbalance and a geometric stiffness imbalance on the behavior of a single lap joint.

### 5.4.1 Material Stiffness Imbalance

In order to simulate a material stiffness imbalance in the adhesive joint, the material properties for the upper adherend were decreased by 30% and 70% of the material properties of the lower adherend. These joints were then compared to a balanced joint. Figure 5.13 shows the joints used for this study.

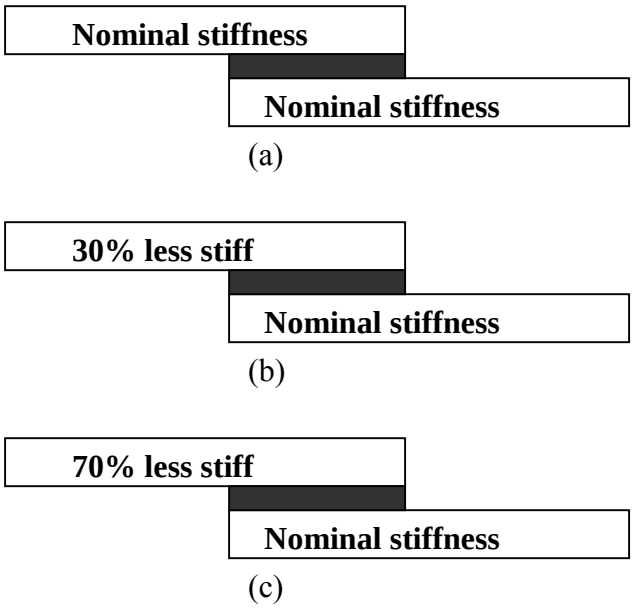


***Figure 5.13: (a) balanced joint, (b) 30% imbalanced joint, and (c) 70% imbalanced joint***

Table 5.2 shows the material properties used.

**Table 5.2: Material Properties for Stiffness Imbalance**

| Mat. Prop | Balanced joint | 30% less stiff | 70% less stiff |
|---|---|---|---|
| Ex (Msi) | 2.16 | 1.512 | 0.648 |
| Ey (Msi) | 1.5 | 1.05 | 0.45 |
| Ez (Msi) | 3.94 | 2.758 | 1.182 |
| Gxy (Msi) | 0.81 | 0.567 | 0.243 |
| Poisson's Ratio | 0.28 | 0.196 | 0.084 |

A stiffness imbalance affects the adhesive more so that the previous parametric cases. Typically, the majority of the load is transferred through the edges of the adhesive layer. Thus both critical areas in the adhesive experience the same stress state. When a stiffness imbalance is created, the maximum shear stress in the adhesive shifts to the critical area from which the less stiff adherend extends. Figure 5.14 shows this shift in shear stress for an increase in stiffness imbalance. The three strips in the figure are the adhesive layers for each case. As seen in the figure, the highly stressed region (yellow area) shifts towards the softer adherend as the imbalance is increased. Also note that the distortion in the adhesive is greatest with the 70% imbalance.

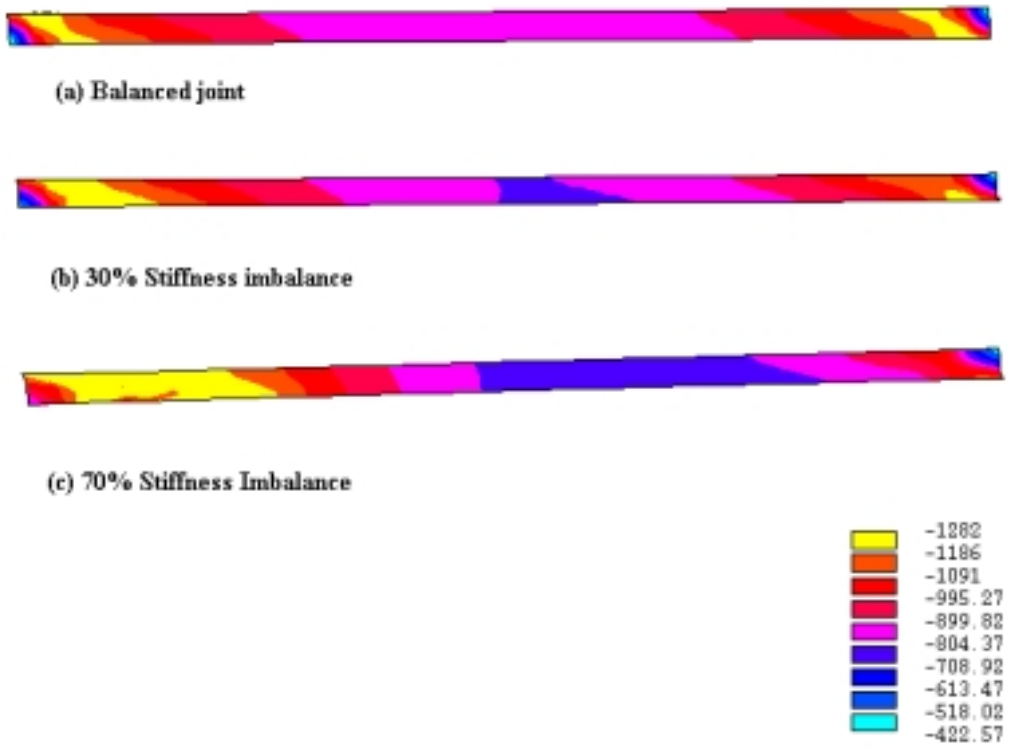


***Figure 5.14: Contour Plot of Adhesive Shear Stress***

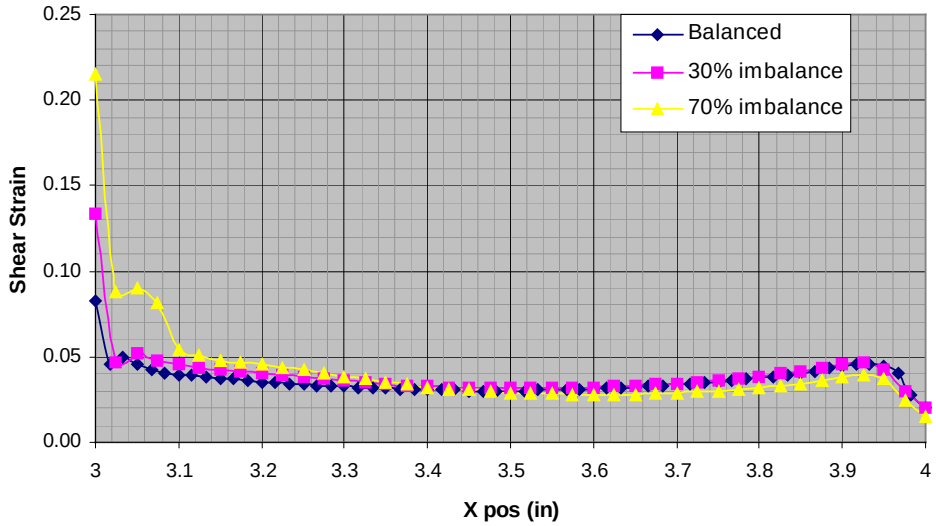


This distortion is evidence of greater differential shearing at the less stiff adherend. As a result, the shear strains are increased as shown in figure 5.15.

***Figure 5.15: Shear Strain in Adhesive layer for Increasing Stiffness Imbalance***

As described in earlier chapters, a large amount of elements is required to accurately obtain the shear strains at the corner of the adhesive (x=3,4). While the mesh cannot be sufficiently refined, a trend can be seen. There is a significant increase in shear

strain between the 70% imbalanced joint and the remaining two joints near the critical edge.

A trend can also be seen in the shear stress distribution of the adhesive as the imbalance is increased as seen in figure 5.16. As the imbalance is increased, the adhesive experiences more yielding. As the amount of yielding is increased, the shear stress tends to flatten out.

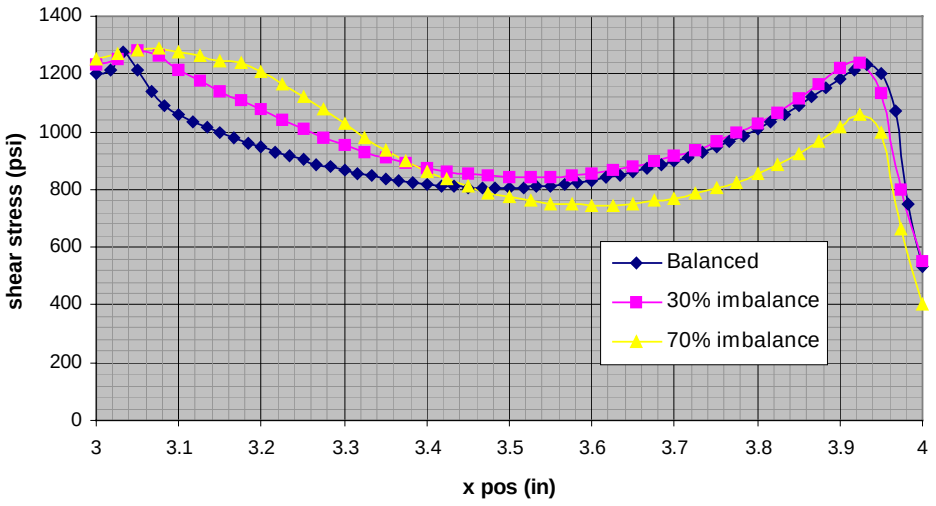


***Figure 5.16: Adhesive Shear Stress for Stiffness Imbalance***

Table 5.3 shows the amount of yielding at the critical area in percent of total area of the adhesive. This critical area coincides with the left side of the adhesive in figure 5.14 where the shear stress is at a maximum. Note that between a balanced and 30% imbalanced joint, the difference is small. However, a 70% imbalance results is a dramatic increase in adhesive yielding.

**Table 5.3: Amount of yielding in adhesive for increasing Stiffness Imbalance**

| Joint Type | Adhesive Yielding |
|---|---|
| No Imbalance | 4% |
| 30% Imbalance | 5% |
| 70% Imbalance | 20% |

The effect this has on the adherends is that the maximum principal stress distribution is shifted over to the critical area, causing it to become overloaded. In all three cases, the upper and lower adherends are experiencing similar stress magnitudes. However, because the stiffness properties are reduced in the upper adherend, it is experiencing a more severe stress state. For an increase in stiffness imbalance, the stresses in the both the upper and lower adherends for all three cases remain the same. However, since the upper adherend becomes less stiff, it is actually in a more critical stress state. In general, a decrease in stiffness causes a decrease in strength of a material. Figure 5.17 shows the transition of the maximum principal stress towards the more critical area.

(a) Balanced joint

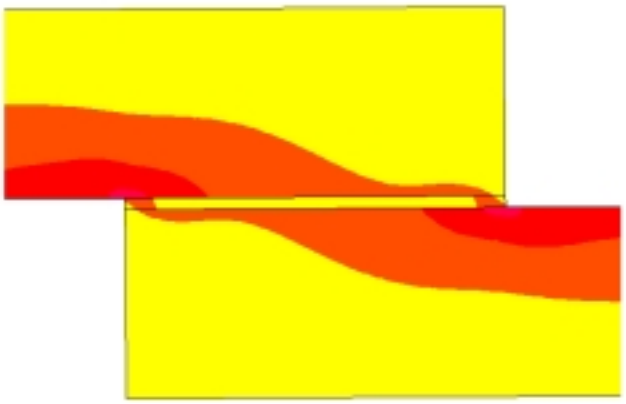

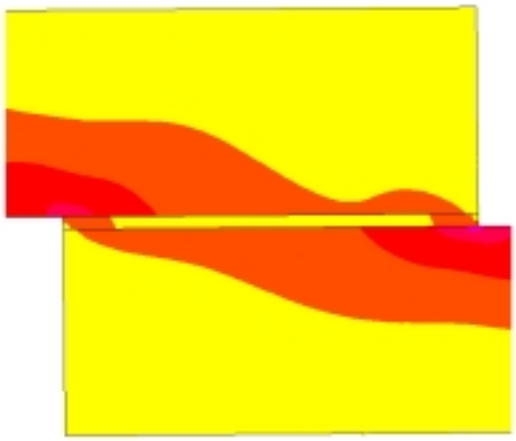

***Figure 5.17: Transition of principal stress towards critical area in upper adherend***

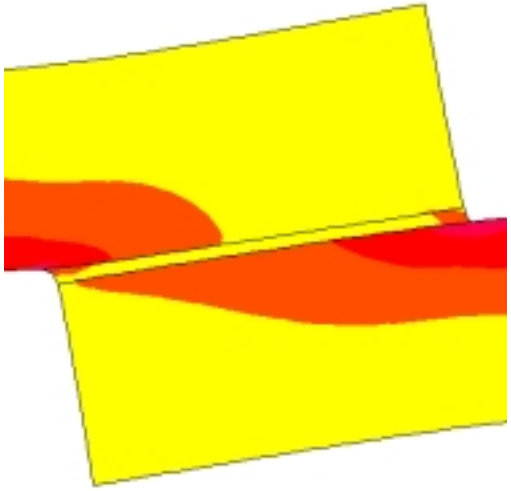

(b) 30% imbalance

(c) 70% imbalance

***Figure 5.17 (continued)***

The yellow area of figure 5.17 represents a very low stress area. As the imbalance is increased, the contours of higher stress (orange and red) shift over to the critical area in the upper adherend.

In terms of the adhesive, a material stiffness imbalance of around 30% will not affect the adhesive too much. However, the adherend is more severely stressed. As the amount of imbalance is increased, the adhesive experiences a progressively adverse stress state.

### 5.4.2 Geometric Stiffness Imbalance

A geometric stiffness imbalance was created by reducing the thickness of the upper adherend by 30% and 70% of the lower adherend as see in figure 5.18.

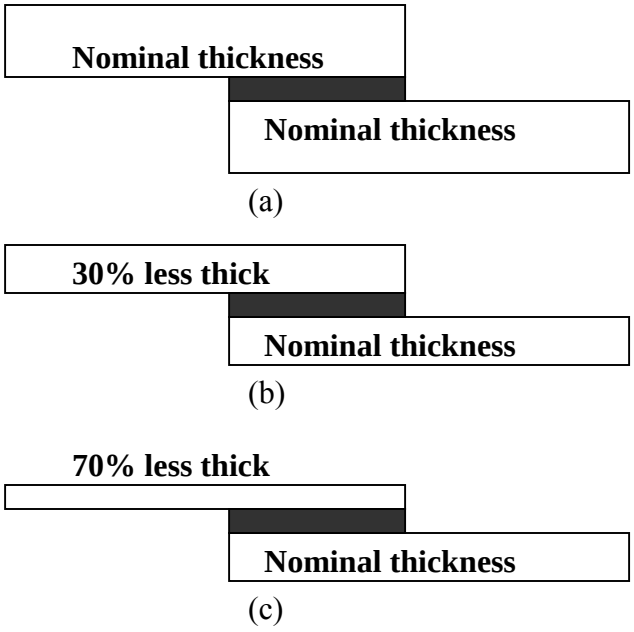


***Figure 5.18: (a) balanced joint, (b)30% thickness imbalanced joint and (c) 70% thickness imbalanced joint***

Table 5.4 lists the thickness of the upper adherend in each case.

**Table 5.4: Thickness of upper adherend with increasing thickness imbalance**

| Joint Type | Adherend Thickness |
|---|---|
| Balanced | .5 inches |
| 30% thickness imbalance | .35 inches |
| 70% thickness imbalance | .15 inches |

As in the material stiffness imbalances joints, the end from which the thinner adherend extends becomes overloaded in the critical area as the majority of the load is shifted here. However, unlike the material stiffness imbalanced study, the adhesive is not as affected by the thickness imbalance. Figures 5.19 and 5.20 show the adhesive peel and shear stress with an increasing thickness imbalance. The stresses are taken along the upper bond line interface. The applied load is 950 lbs.

***Figure 5.19: Shear Stress distribution in adhesive layer for increasing thickness imbalance***

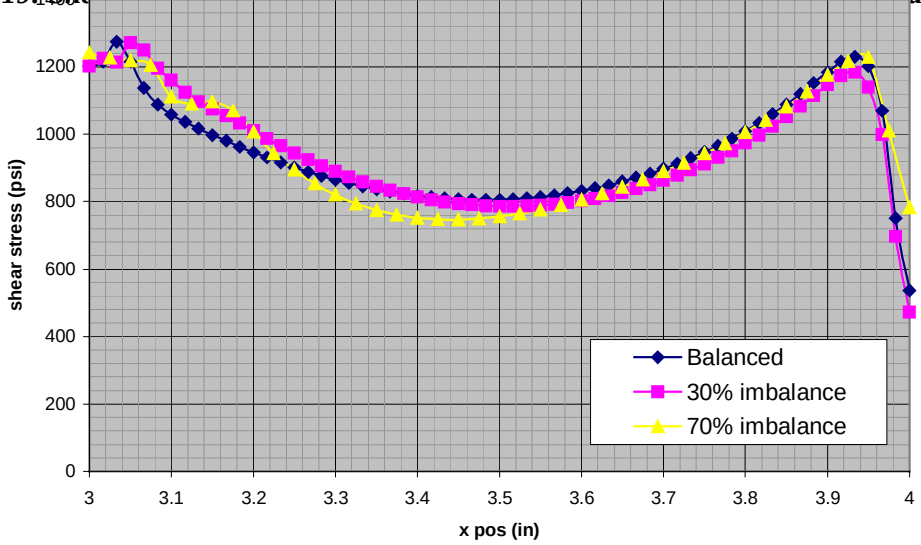

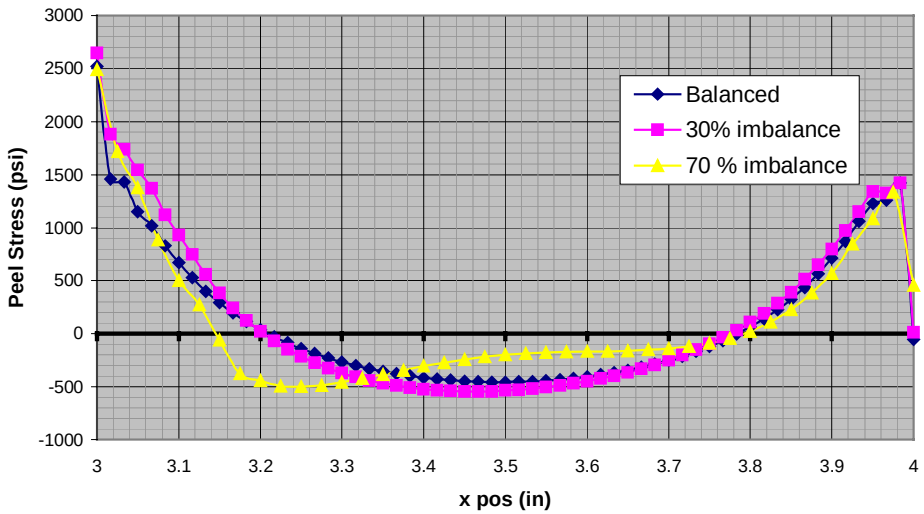


***Figure 5.20: Peel Stress distribution in adhesive layer for increasing thickness imbalance***

While the middle region for the peel stress distribution in the 70% imbalance case is different from the balanced and 30% imbalanced cases, this is not the critical region where heavy load is transferred from one adherend to the other. Looking at the edges of the adhesive, there is no significant difference between the cases.

The Tsai failure criterion gave a failure load of 750 and 500 lbs for the 30% and 70 % imbalanced joints respectively and 950 lbs for the balanced joint. For both the 30% and 70% imbalanced joints, the adhesive experienced shear strains between 3% and 5% at these failure loads. Thus the adhesive is not an area of concern for failure in the sense that the composite will most likely fail first.

When the thickness of one adherend is changed, there are geometric as well as material stiffness effects that affect the joint behavior. For a beam under uniaxial tension the stress is given as P/A where P is the applied force and A is the cross-sectional area.

For the same load P, the stress will increase as the area is decreased. Essentially, that is what happens with a thickness imbalanced joint. Figure 5.21 shows the contour plots of the first principal stresses for each case. As the thickness of the upper adherend is

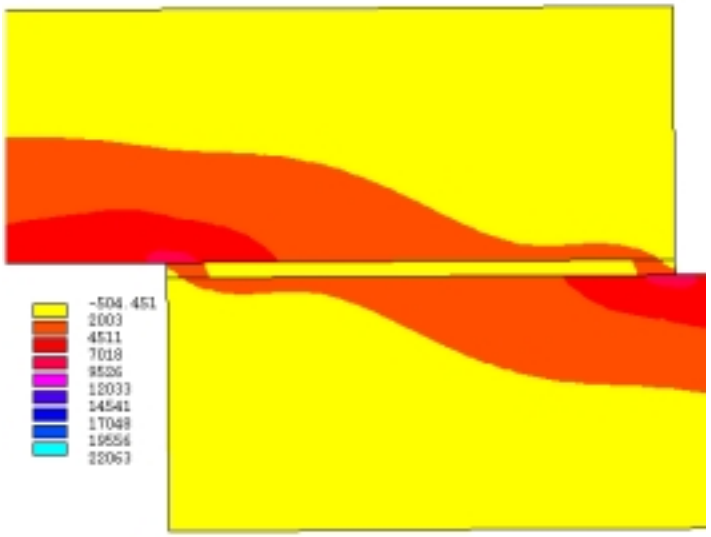


decreased, the stresses at the critical area increase. Note also that the less critical end of the adhesive experiences a decrease in stress as the imbalance is increased.

(a) Balanced joint

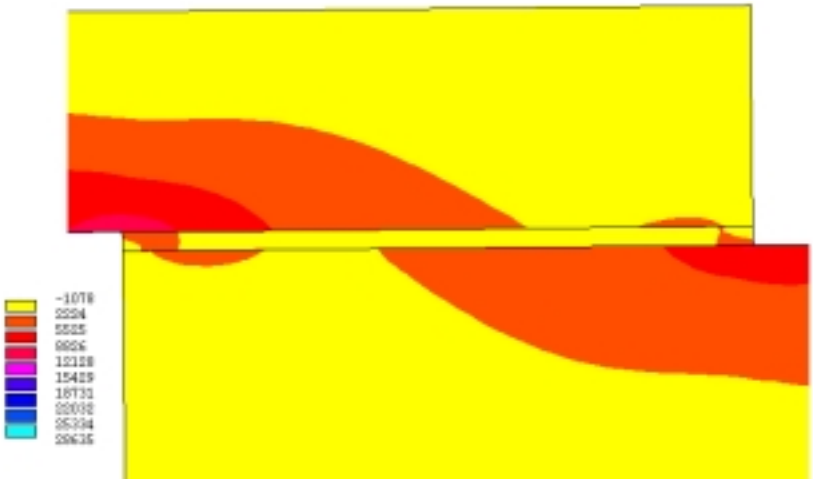

(a) 30% thickness imbalance

***Figure 5.21: Principal Stress distribution in a (a) Balanced joint (b) 30% imbalanced joint and a (c) 70% imbalanced joint***

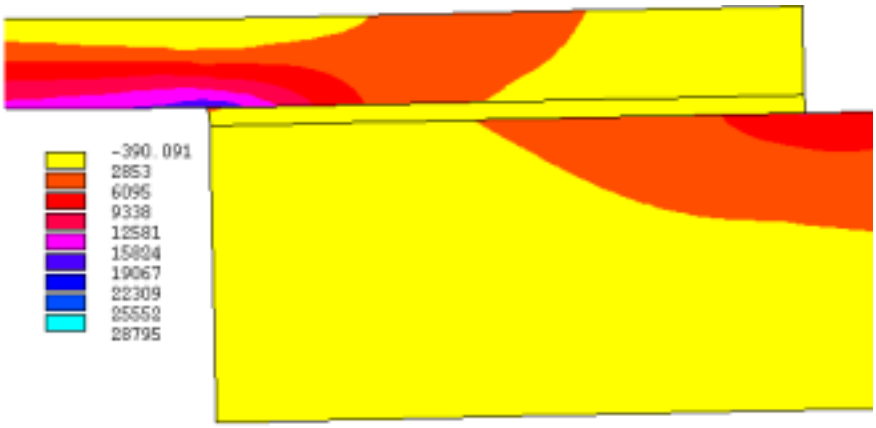


(c) 70% thickness imbalance

***Figure 5.21 (continued)***

As expected, the stresses will increase as the thickness of the upper adherend is decreased. Figure 5.22 shows the ratio of the maximum principal stress in the upper adherend for each case verses the maximum stress in the balanced case.

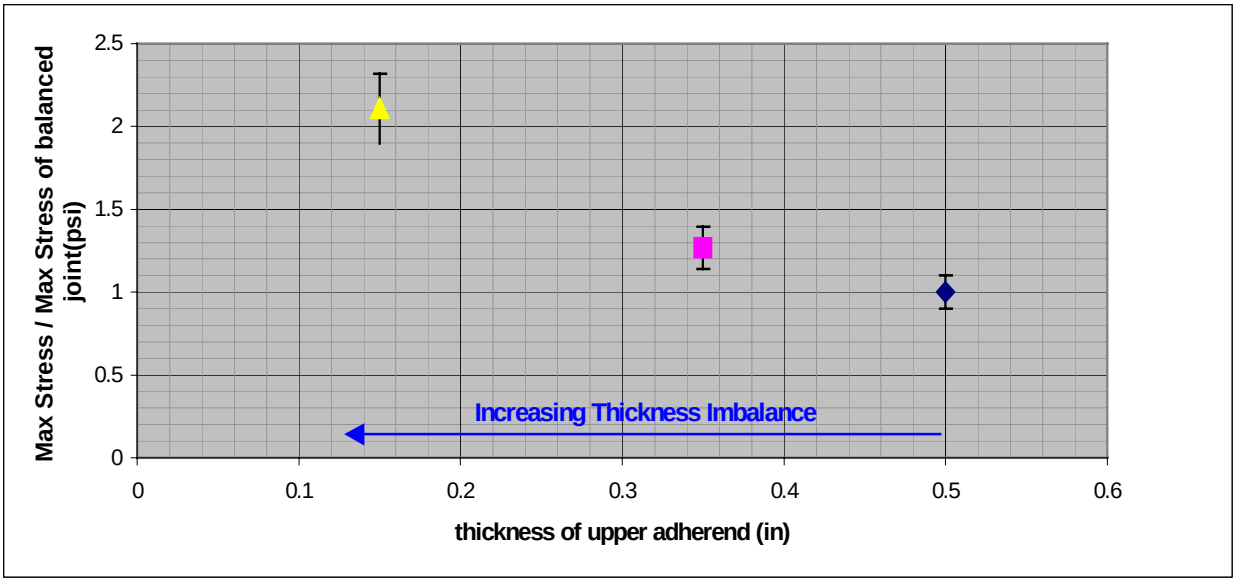


***Figure 5.22: Ratio of maximum stress in upper adherend verses the maximum stress in balanced joint***

Another characteristic of increasing the thickness imbalance is that the difference between the average stress in the upper adherend away from the bond and the maximum stress experienced near the bond is decreased. That means that as the thickness imbalance is increased, the entire thinner adherend becomes highly stressed. The more balanced the joint is, the more localized the stress concentration becomes. In order to illustrate this point, figure 5.23 shows a plot of the ratio of the maximum principal stress experienced in the thinner adherend verses the average principal stress experienced in that adherend away from the joint.

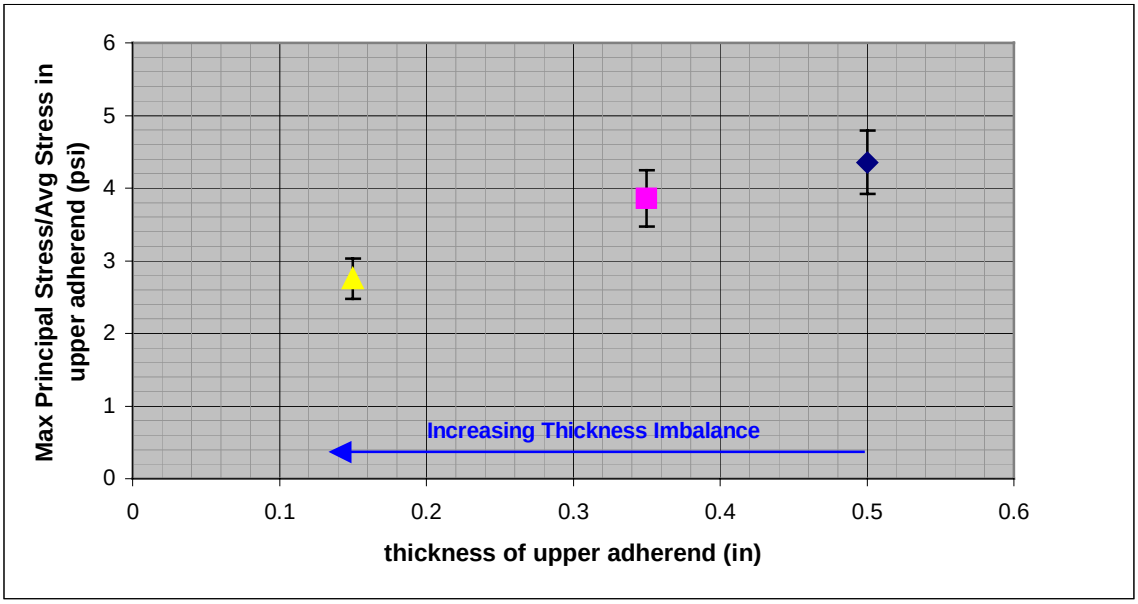


***Figure 5.23: Ratio of maximum principal stress to average stress in upper adherend***

As the thickness is decreased, the ratio becomes smaller.

In conclusion, a thickness imbalanced joint does not significantly affect the adhesive. Rather the critical component to consider is the adherend. As the thickness imbalance is increased, the effect this imbalance has on the stress state of the thinner adherend becomes more severe.

# 6. Physical Testing

While the finite element models proved to be useful for a parametric study, physical tests were needed in order to investigate interfacial issues associated with different types of adhesives and different types of laminates. Single lap joints were made and tested in uniaxial tension in accordance with ASTM standard D 5868-95 [11]. Every test was conducted at North Carolina State University using an Instron 4400 Series testing machine.

ASTM standard D 5573-99 [12] classifies failure modes in FRP joints into seven different classes. The first class is adhesive failure (also called interfacial failure) where the separation of the joint is between the adhesive and the adherend. After failure, one adherend has the entire adhesive layer attached while the other adherend contains no adhesive. The second class, called cohesive failure, occurs when the separation of the joint is within the adhesive layer. After failure, both adherends have part of the adhesive layer attached. Similar to a cohesive failure is a thin-layer cohesive failure. This type of failure occurs when the failure is still within the adhesive layer but the majority of the adhesive is on one adherend. The other adherend has just a light layer of adhesive attached. The fourth class is called a fiber-tear failure. This describes failure when separation is within the FRP matrix only. Reinforced fibers are on both ruptured surfaces. Light-fiber-tear failure is the same as fiber-tear failure except that failure occurs near the surface of the adherend/adhesive interface. Little or no fibers are transferred from the adherend to the adhesive layer. The sixth class is called stock-break failure. This occurs

when the separation is within the adherend but outside the bonded region. The last class is called mixed failure where the failure is a mixture of different classes.

The main classes experienced by the physical tests performed were adhesive failure, thin-layer cohesive failure and fiber tear.

## 6.1 Reichhold Inc.

The first set of tests consisted of adherends 4.0 inches long, 1.0 inch wide and 0.5 inch thick. The bonded area was 1.0 square inch with an adhesive thickness of 0.03 inches. Three different adherend laminates were tested, each with a different surface layer. The different surface layers were investigated in order to determine the effects the added layer would have on the adhesive/adherend interface as well as to understand the actual behavior of the bonded joint. The added surface layer was desired in the laminate because it simplifies the pultrusion process. An added layer of continuous thermoplastic fibers, or veil, helps the material pull through the guiding system without tearing out. The veil also protects the underlying glass mat in the composite from water, UV or other chemicals.

The first laminate, labeled No Mat, was the control. No additional fibers were added to the existing composite. The second, labeled 1.5 oz OC, consisted of a layer of continuous strand mat of Owens Corning fibers on the surface. The final laminate, NM 1001, included a continuous strand mat of Nexus fibers on the surface. These layers were added during the pultrusion process.

The adhesive used was POLYBOLT adhesive provided by Reichhold Inc. The adhesive was mixed and applied in accordance with Reichhold Inc. specifications. Once

the adherends were bonded, they were left to cure for 24 hours prior to testing. The results of the tests are summarized in Table 6.1.

**Table 6.1: Test Results using Reichhold Adhesive**

| *Specimen* | *Max Stress* | *Failure Mode* |
|---|---|---|
| No Mat-A | 1557 | Adhesive |
| No Mat-B | 1376 | Adhesive |
| No Mat-C | 1374 | Adhesive |
| No Mat-D | 1191 | Adhesive |
| **average** | **1374** | |
| 1.5 oz OC-A | 1279 | Adhesive |
| 1.5 oz OC-B | 1250 | Adhesive |
| 1.5 oz OC-C | 917.6 | Adhesive |
| 1.5 oz OC-D | 1203 | Adhesive |
| **average** | **1162** | |
| NM 1001-A | 1261 | Adhesive |
| NM 1001-B | 1410 | Adhesive |
| NM 1001-C | 1437 | Adhesive |
| NM 1001-D | 1024 | Adhesive |
| **average** | **1283** | |

In every case, the failure mode was adhesive failure. Figure 6.1 shows the bonded region of both adherends. After failure, there is no evidence that the adhesive or adherend

transferred over to the other. Rather, the surface of both the adherend and adhesive appears shiny which indicates that the adhesive "slipped off" the adherend.

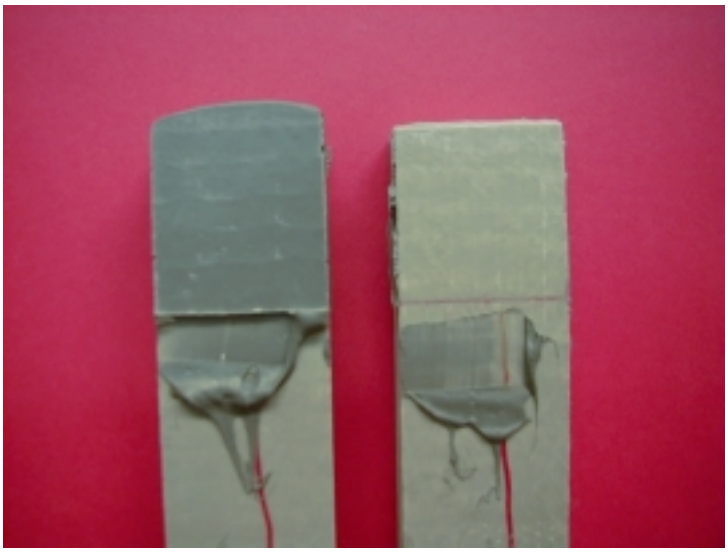

***Figure 6.1: Failure of a single lap joint using POLYBOLT adhesive***

In a well-designed joint, the adhesive should permeate into the composite matrix, creating a strong interface. This bonded area should be the last to fail. Therefore, an adhesive failure was not desirable. In addition to a poor failure mode, the maximum applied load was very low. A failure load of at least 1800 lbs was expected based on previous experiments performed by MMC on different adhesives. Because the control specimens (No Mat) experienced adhesive failure as well, it was concluded that the adhesive and not the laminate surface, was unacceptable. Therefore a different adhesive with better properties was desired.

## 6.2 Ashland Chemical-1

Using the same type of laminate specimens from the previous tests, PLIOGRIP® structural adhesive from Ashland Chemical was used for bonding. Once the adhesive was applied, the joints were cured for 24 hours. The results are summarized in Table 6.2.

**Table 6.2: Test Results using Ashland Adhesive**

| Specimen | Max Load (lbs) | Failure Mode |
|---|---|---|
| No Mat | 2062 | Fiber Tear |
| No Mat | 2263 | Fiber Tear |
| **average** | **2163** | |
| 1.5 oz OC | 2477 | Adhesive and cohesive failure |
| 1.5oz OC | 2198 | Adhesive and cohesive failure |
| **average** | **2338** | |
| NM 1001 | 2096 | Thin-layer cohesive failure |
| NM 1001 | 1646 | Thin-layer cohesive failure |
| **average** | **1871** | |

Fiber tear failure is the most desirable failure mode because it indicates that the adhesive bond is stronger than the composite.

As seen in Table 6.2, the mode of failure changed for each laminate group as well as the failure load. Figure 6.2 shows the bonded area after failure for each laminate group.

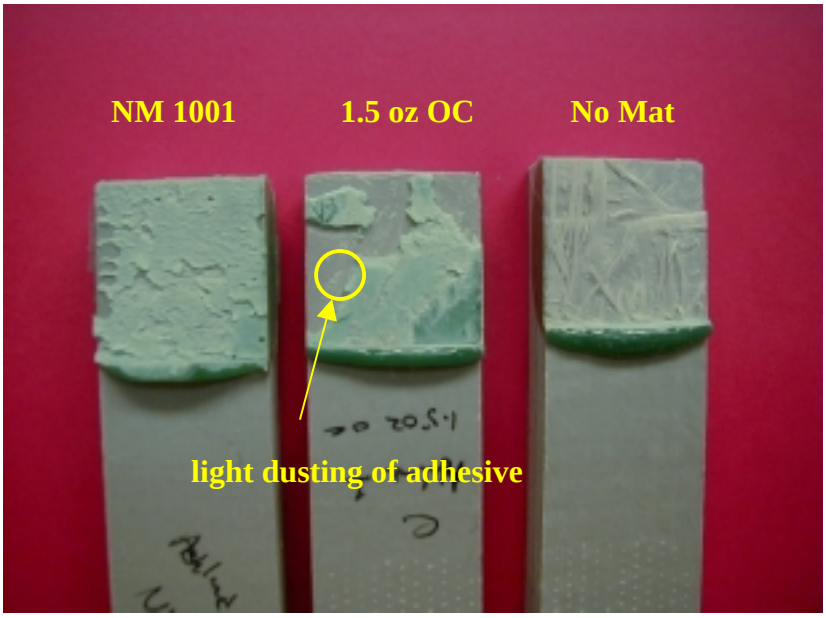


***Figure 6.2: Failure of different laminates using PLIOGRIP® adhesive***

Note the difference between the surfaces of each specimen. For the NM 1001 laminate, the surface is rough indicating that the separation occurred within the adhesive. The 1.5 oz OC laminate is a combination of cohesive and adhesive failure. The majority of the adhesive surface is smooth, indicating that it "slipped" off the opposite adherend. However, there is some evidence of a "light dusting" of adhesive on the adherend surface as indicated by figure 6.2. The No Mat laminate experiences total fiber tear. The adhesive layer is completely intact and all of the failure occurs within the laminate.

By changing only the surface layer within the laminate, the behavior of the joint is changed significantly. It was concluded that the surface layer plays a critical role in the failure mode and failure load of a bonded joint.

While the failure mode for both the NM 1001 group and 1.5 oz OC group was still predominately due to the adhesive layer, the maximum load to failure was well

within the acceptable range determined by MMC. It was also concluded that an added layer of nexus continuous strand mat would not adversely affect the adherend/adhesive interface beyond the acceptable range and would ease the pultrusion process.

## 6.3 Ashland Chemical-2

With the nexus layer included in the pultruded composite, new specimens were cut from the upper and lower flanges of the MMC bridge deck for further testing. All specimens were cut to be 4.0 inches long and 1.0 inch wide. The bonded area was 1.0 inch wide by 1.0 inch long with an adhesive thickness of .03 inches. The upper adherend had a nominal thickness of 0.32 inches while the lower adherend had a nominal thickness of 0.35 inches. Also, due to the location of the cut, the upper adherend included areas of thicker sections. These “bumps”, illustrated in figure 6.1, are primarily for stiffening critical parts in the bridge deck.

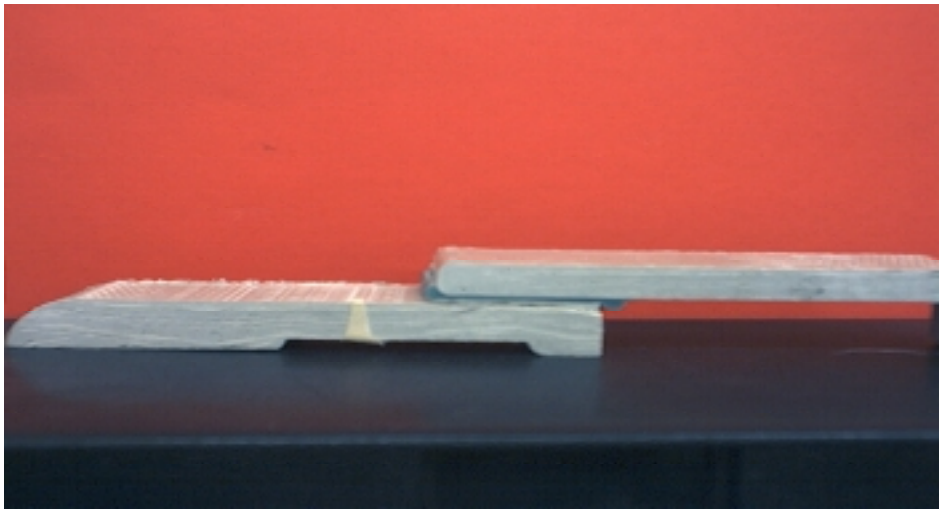

***Fig. 6.1: Lap Shear Specimen with bumps***

Once applied, the adhesive was allowed to cure for three days. The cure time was increased from that of the Ashland Chemical-1 tests in order to determine its effect on the behavior of the bond.

Three different scenarios were tested. The first scenario involved joining the specimens as they were. It was not clear how the varying thickness of the one adherend affected the joint behavior. Therefore a second testing scenario was conducted with the bumps machined off. As seen in table 6.3, the bumps increased the maximum load capacity of the joint.

The third testing scenario involved offsetting the grips on the Instron machine so that they did not apply any unwanted bending moments on the adherends. In a typical test setup, the grips on the Instron are colinear. In a single lap joint, the centers of the adherends are offset by at least one adherend thickness plus the thickness of the adhesive. While the upper grips are attached to a universal joint, allowing them to slightly shift horizontally, the adherends still had to be forced into them. Because the grips and the adherends were not perfectly aligned, a bending moment was applied to the ends of the adherends. The effect of this moment was not known. In order to eliminate this moment, the lower grips were mounted on a plate that allowed them to slide horizontally until the grips were directly in line with the appropriate adherend. Table 6.4 lists the results from the three tests.

**Table 6.4: Testing Results using Ashland Adhesive. Composite includes Nexus Fibers.**

| *Specimen* | *Max Load (lbs)* | *Mode of Failure* |
|---|---|---|
| Normal-1 | 1721 | Fiber tear |
| Normal-2 | 1678 | Fiber tear |
| Normal-3 | 1583 | Fiber tear |
| Normal-4 | 1757 | Fiber tear |
| Normal-5 | 1429 | Fiber tear |
| **Average** | **1634** | |
| No Bump-1 | 1427 | Fiber tear |
| No Bump-2 | 1440 | Fiber tear |
| No Bump-3 | 1506 | Fiber tear |
| **Average** | **1458** | |
| Offset-6 | 1734 | Fiber tear |
| Offset-7 | 1541 | Fiber tear |
| **Average** | **1638** | |

The results indicate that the grips in their original position do not have an adverse affect on the strength of the joint. Also, by comparing the failure modes from the two different Ashland tests, a longer cure time gave a stronger, more efficient bond.

# 7. Interface and Surface Preparation Testing

Surface preparation can have a significant effect on the maximum load capacity of a bonded joint. A study was carried out on a butt-strap joint to better understand how critical surface preparation can be. A butt-strap joint was chosen rather than a singe lap joint due to its similarity to the field joints installed on the MMC FRP bridge deck as described in chapter 1. It was desired to better understand the effects surface preparation had on these field joints. Simulating this field joint and performing this study provided immediate answers to these effects. A typical butt-strap joint consists of two adherends connected by a strap, as shown in figure 7.1.

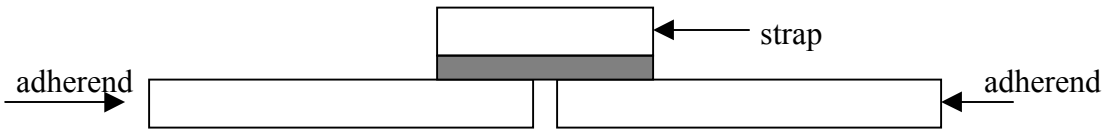


***Figure 7.1: Butt-Strap Joint***

The butt-strap joint used for this analysis consisted of two MMC composite adherends bonded together by one layer of triax continuous strand mat. This is a fabric consisting of three layers of fibers oriented at 0º, 45ºand 90 º from the longitudinal direction. The mat was bonded onto the composite by ATLAC® 580-05 urethane-modified vinyl ester resin provided by Reichhold Chemicals, Inc. The resin was prepared in accordance with ATLAC® specifications. Once applied, the butt-strap joint was left to

cure for two days. After that time, it was tested in the Instron testing machine under uniaxial tension. Figure 7.2 shows three specimens after they have been cured.

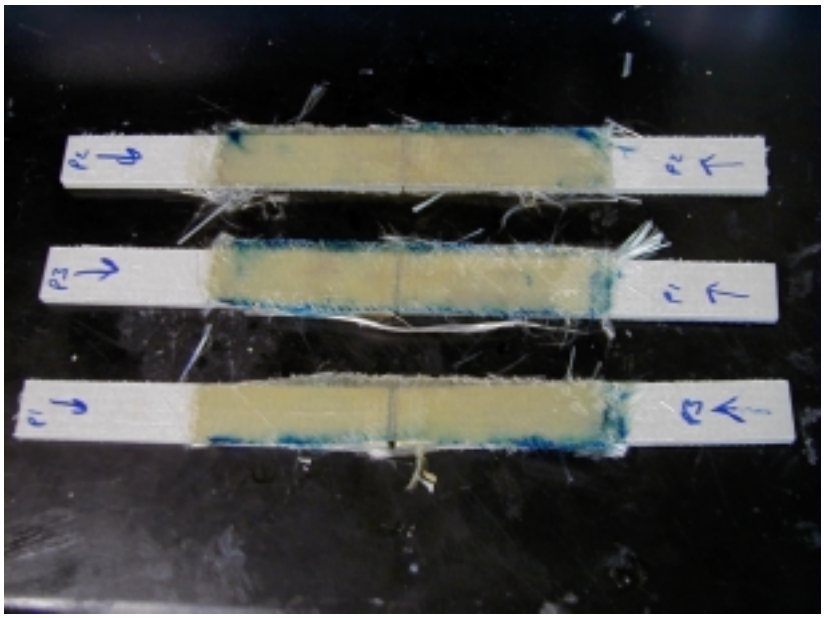

***Figure 7.2: Butt-strap joints***

Three types of surface preparations were performed. The first was an acetone wipe on the surface of the MMC composite adherends using a cotton swab. The second involved sanding the adherends with sand paper, followed by an acetone wipe. The specimens were sanded with 360 grit wet or dry sand paper. They were sanded until the surface was no longer shiny. The third surface preparation involved an acetone wipe followed by the application of ATPRIME® 2, a secondary bonding agent provided by Reichhold Inc. The ATPRIME® 2 is a two-component urethane-based primer system which was developed to enhance adhesion to FRP in secondary laminating operations. A secondary laminating operation can be described as creating a laminate on top of an

existing laminate. For these tests, bonding a layer of triax with resin onto the MMC composite adherends constitutes a secondary laminating operation. The primer was prepared according to Reichhold specifications. Once it was prepared, a layer was applied by brushing it onto both adherends and allowed to dry for 24 hours. The adherends were wiped with acetone before the application of the primer. The ATPRIME® 2 was sufficiently dry when it could not be indented by a fingernail. The layer of triax was then applied in the same manner as the other cases and allowed to cure for two days. The results of the tests are shown in table 7.1.

**Table 7.1:Results from butt-strap tests**

| Specimen | Failure Load | Failure Mode |
|---|---|---|
| Acetone1 | 300 | interface |
| Acetone2 | 465 | interface |
| Acetone3 | 213 | interface |
| Acetone4 | 333 | interface |
| **average** | **328** | |
| Sanding1 | 1535 | interface |
| Sanding2 | 1496 | interface w/ light fiber tear |
| Sanding3 | 1604 | interface w/ light fiber tear |
| Sanding4 | 1357 | interface |
| **average** | **1498** | |
| Atprime-1 | 2064 | fiber tear |
| Atprime-2 | 2622 | fiber tear |
| Atprime-3 | 2469 | fiber tear |
| **average** | **2385** | |

Looking at just the loads to failure, by simply sanding the adherends, the maximum load to failure is increased by 350%. When the adherends are sanded, the matrix is broken up slightly, allowing the resin to permeate deeper into the composite as compared to an acetone wipe.

The failure mode for both the acetone wipe and the sanded group was interfacial failure. The strap experienced a clean break from the adherend as shown in figure 7.3.

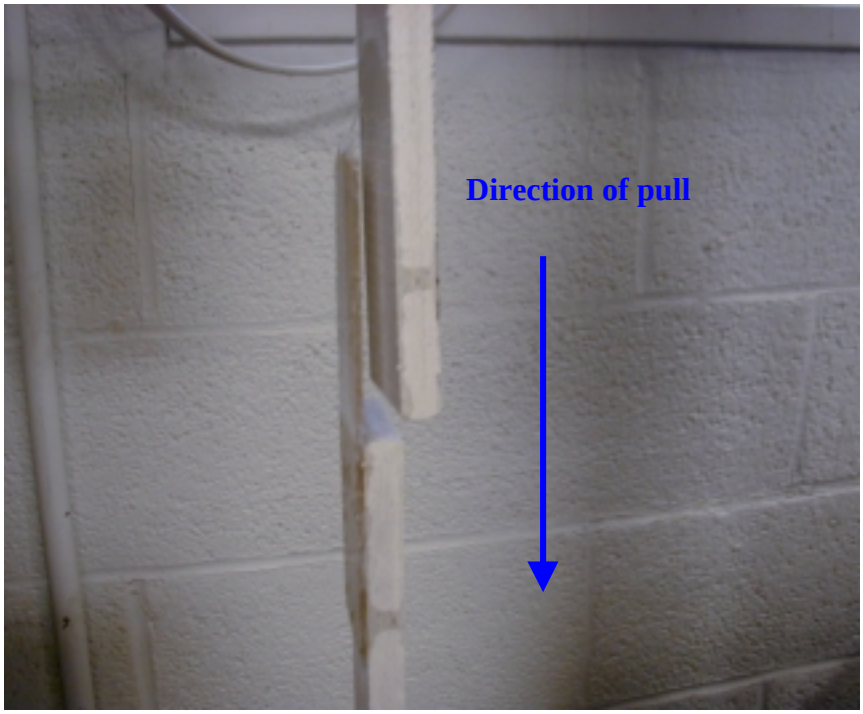


***Figure 7.3: Failure mode for the acetone wipe and sanded specimens***

One major difference between the two groups was that the sanded group experienced light fiber tear. Figure 7.4 shows the surfaces of the adherend and the strap after failure for the acetone wipe group and the sanded group.

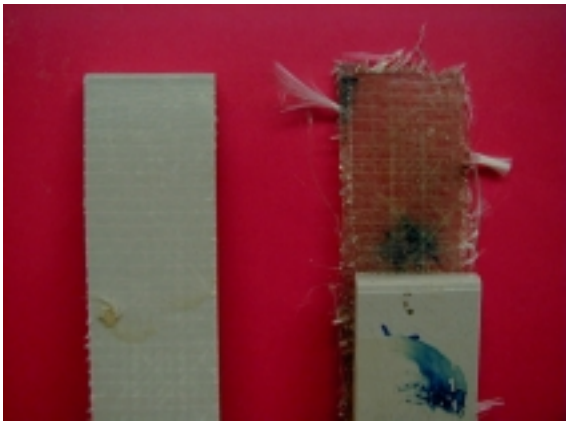

(a) Acetone wipe specimen

(b) Sanded specimen

***Figure 7.4: Interface after failure for the (a) acetone wipe group and the (b) sanded group***

Notice the surface of the adherend in 7.4(a) is shiny as compared to the dull surface of the adherend in 7.4(b). In addition, the strap has a light "dusting" of fibers on its surface. As described earlier, the resin was better able to seep into the matrix of the composite for the sanded specimens. For the acetone group, the interface was very weak with no evidence of the resin bonding to the composite properly.

The ATPRIME® bonding agent yielded the best results by far. The maximum load to failure was increased by 60% from the maximum given by the sanded group. In addition, the failure mode was total fiber tear as seen in figure 7.5.

***Figure 7.5: Interface after failure for specimens with ATPRIME®***

In conclusion, surface preparation is critical with respect to the performance of a bonded joint. While this can be the most difficult to control in real world applications, care should be taken to properly prepare the surface of the bonding area so that the joint can perform at its optimum level.

# 8. Conclusions and Recommendations

## 8.1 Conclusions

The purpose of this research was to analyze adhesively bonded FRP joints. This was accomplished by first developing a finite element model of a single lap joint for a parametric study. This model was compared with theory in order to verify the results. Then, physical tests were performed on single lap joints using MMC FRP adherends and two different structural adhesives. Finally, physical tests on butt-strap joints were performed in order to investigate the effects different surface preparations had on the behavior of the joint.

The parametric study led to the following conclusions:

1. Adding a taper to a single lap joint increases the magnitude of stress at the critical area of the adherends. The adhesive peel and shear stresses at this area are not significantly affected. Therefore a taper is not recommended for a single lap joint.
2. A convex or a concave fillet at the edge of the adhesive layer slightly decreases the magnitude of stress in the critical areas of the adherends. In addition, a concave fillet will significantly reduce the peel and shear stresses in the adhesive layer at the edges. Therefore, a concave fillet is the most desirable edge shape for the adhesive layer.

3. A material stiffness imbalance causes the adhesive to overload the critical side of the adherend. Therefore, the less stiff adherend is in a more severe stress state. In addition, the adhesive experiences a greater amount of yielding with a greater stiffness imbalance. The more the adhesive yields, the sooner it will fail. While a 30% stiffness imbalance did not show a significant difference in the amount of adhesive yielding, the adherend is more severely stressed. Therefore both the adherend and adhesive need to be considered if a material stiffness imbalanced joint is to be created.
4. A geometric stiffness imbalanced joint predominantly affects the adherends. The adhesive stresses are not significantly altered. As the thickness of one adherend is decreased, the entire adherend becomes highly stressed. With a balanced joint, the high stress concentration is localized at the edges of the bonded area.

The physical tests performed on the single lap joint and the butt-strap joint yielded the following conclusions:

1. POLYBOLT structural adhesive was not satisfactory for use with MMC composite panels due to a weak interface and a low failure load.
2. By changing the surface layer in the laminate during manufacturing, the mode of failure of the joints was changed.
3. By increasing the amount of curing time for the adhesive, the mode of failure for the NM 1001 specimens was changed to a fiber tear failure. This is the most desirable failure mode.

4. By sanding the surface of the adherends of the butt-strap joint before bonding, the maximum load capacity is increased by 350% from that of an acetone wipe surface preparation.
5. ATPRIME® bonding agent provided by Reichhold Inc. gave the highest load to failure and a fiber tear failure mode. This surface preparation gave the best joint performance.

## 8.2 Recommendations

While this research provided much information regarding adhesively bonded joints, more work is needed to design a structural splice for the MMC FRP bridge deck. One concept for a design was a tube joint where layers of material are cured onto the existing composite within the cells of the bridge. Figure 8.1 shows a preliminary sketch of this concept.

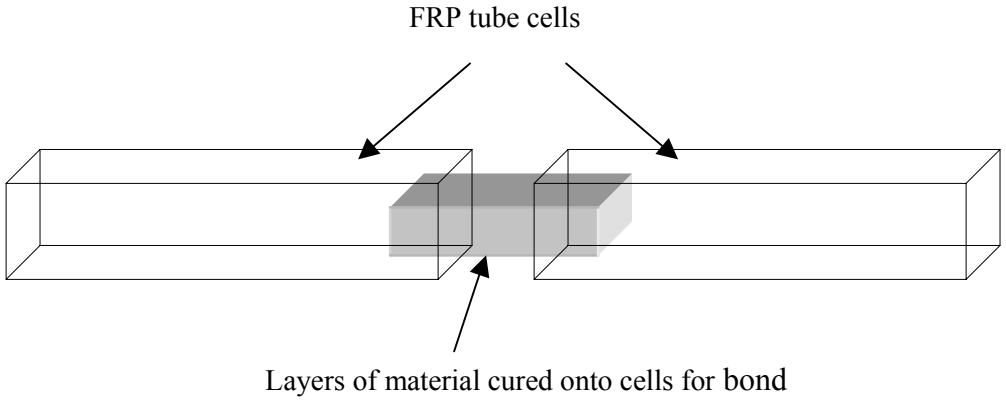


***Figure 8.1: MMC splice concept***

The layers of material are wrapped around the inside diameter of the tube to form a tubular joint. The resin used to cure this material is used as the adhesive that joins the two cells together. The challenge of this design is how to apply the layers of material in the tube. The tubes can be up to 10 feet long, making it difficult to apply the material and resin to form the bond. One idea is to use a type of balloon that expands through both cells and holds the material and resin in place while it cured. Further development is needed with this concept.

## References


1. Adams, R.D., J Comyn, and W.C. Wake. Structural Adhesive Joints in Engineering: Second Edition. London: Chapman & Hall, 1997.

2. Volkersen V.O. "Die Nietkraftverteilung in zugbeanspruchten Nievtverbindungen mit konstanten Laschenquerschnitten." Luftfahrforschung 15 (1938): 41-47.

3. Goland, M., and E. Reissner. "The Stresses in Cemented Joints." Journal of Applied Mechanics Mar. 1944: A-17 – A27.

4. Hart-Smith, L.J. Analysis and Design of Advanced Composite Bonded Joints. NASA CR-2218. McDonnell Douglas Corporation. California: Aug. 1974.

5. Klarbring, A., and A.B. Movchan. "Asymptotic Modeling of Adhesive Joints." Mechanics Of Materials 28 (1998): 137-145.

6. Delale, F., and F. Erdogan. "Viscoelastic Analysis of Adhesively Bonded Joints." Journal of Applied Mechanics 48 June 1981: 331-338.

7. Frostig, Y., O.T. Thomsen, and F. Mortensen. "Analysis of Adhesive-Bonded Joints, Square-End, and Spew-Fillet – Higher Order Theory Approach." Journal of Engineering Mechanics Nov. 1999: 1298-1307.

8. Adams, R.D., N.A. Peppiatt. "Stress Analysis of Adhesive-Bonded Joints." Journal of Strain Analysis 3rd ser. 9 (1974): 185-196.

9. Dattaguru, B., R.A. Everett, J.D. Whitcomb, and W.S. Johnson. "Geometric Nonlinear Analysis of Adhesively Bonded Joints." Journal of Engineering Materials and Technology 106 Jan. 1984: 59-65.

10. Delsen Testing Laboratories, Inc. 1024 Grand Central Avenue Glendale, California 91201-3011. (818) 247-4106.

11. ASTM D 5868-99, Test Method for Lap Shear Adhesion for Fiber Reinforced Plastic Bonding.

12. ASTM D 5573-99, Standard Practice for Classifying Failure Modes in Fiber-Reinforced-Plastic Joints.

13. Allen, K.W. Adhesion 2. Applied Science Publishers. 1978.

14. Budynas, Richard G. Advanced Strength and Applied Stress Analysis. WCB/McGraw-Hill, 2nd ed. USA, 1999.

15. Chamis, C.C., and P.L.N. Murthy. Simplified Procedures for Designing Adhesively Bonded Composite Joints. Proc. of 44th annual Conference of SPI Composites Institute. 6-10 Feb. 1989. Dallas.

16. Hart-Smith, L.J. Non-Classical Adhesive-Bonded Joints in Practical Aerospace Construction. NASA CR-112238, McDonnell Douglas Corporation. California: Jan. 1973.

17. Hyer, M.W., and David Cohen. Calculation of Stresses and Forces between the Skin and Stiffener in Composite Panels. Proc. of AIAA/ASME/ASCE/AHS 28th SDM Conference No. 87-0731.

18. Tong, Liyong and Grant P. Steven. Analysis and Design of Structural Bonded Joints. Boston: Kluwer Academic Publishers, 1999.

19. Delsen Testing Laboratories, Inc.; 1024 Grand Central Avenue, Glendale, California 91201-3011, USA (818) 247-4106

# Appendix A

A single lap joint can be difficult to assemble due to the fact that the adherends tend to slide out of alignment. In addition, the thickness of the adhesive layer needs to be controlled somewhat. These factors were overcome by using the following method.

The joints were prepared in groups of five. The bottom adherends were lined up next to each other separated by thin strips of aluminum. These metal strips spanned the length and width of the joints. There were waxed so that when the adhesive was applied, it would not bond to them. It was important that the strips were rigid enough so as not to flex under the pressure of the grips. The adhesive was then applied to the lower adherends with a plastic knife and spread around the bonded region. This region was one inch wide by one inch long. The upper adherends were then placed on top of the lower adherends to create the single lap joint. The upper adherends were propped up on a surface that was one adhesive thickness higher than the lower adherend. This was accomplished by placing a shim with the desired adhesive thickness on extra composite parts that were the same thickness as the lower adherends. This is illustrated in figure A1.

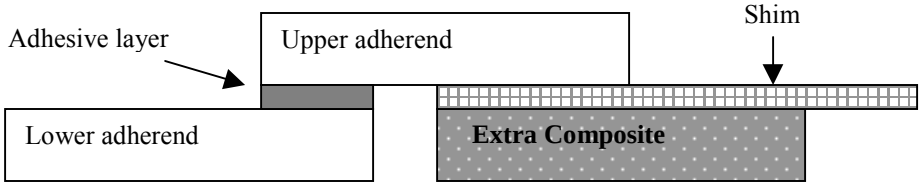


***Figure A1: Preparation of a Single Lap Joint***

Once assembled, grips were applied to the edges of the outside joints. This added pressure forced the adherends into alignment by squeezing them up against the stiff metal strips. A top view of this is shown in figure A2.

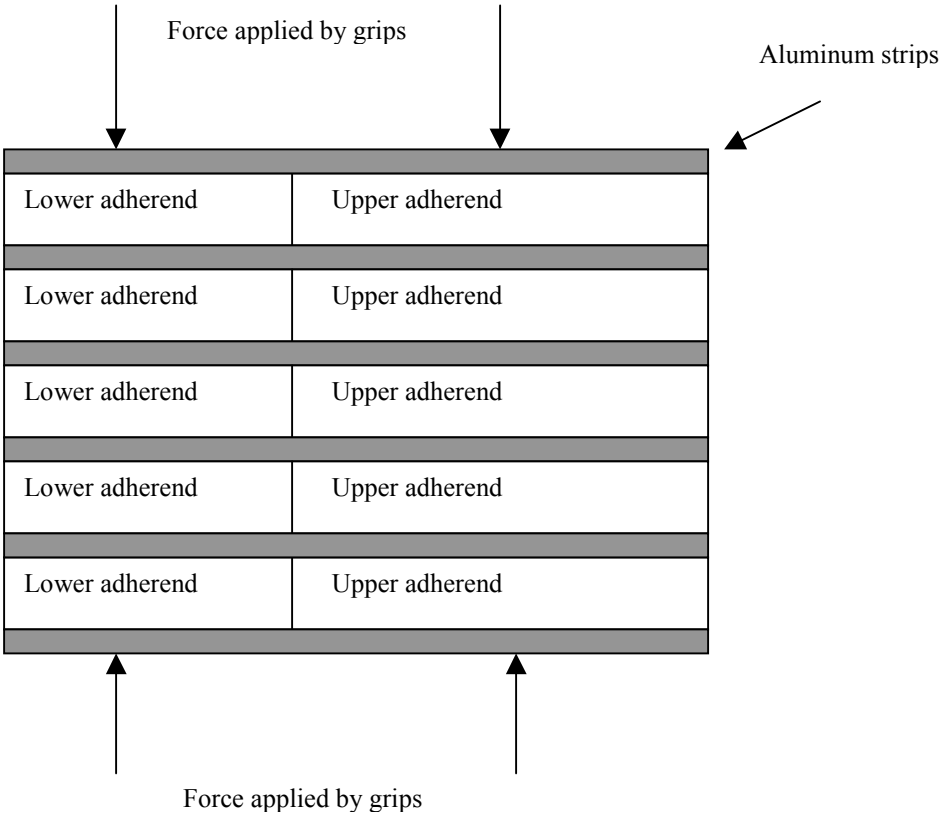


***Figure A2: Top view of the assembled single lap joints***

Depending on the type of adhesive used, the joints were allowed to cure for 1-3 days.